



Review

Manufacturing Functional Polymer Surfaces by Direct Laser Interference Patterning (DLIP): A Polymer Science View

Cesar Alfredo Barbero * and Diego Fernando Acevedo

Research Institute for Energy Technologies and Advanced Materials (IITEMA), National University of Río Cuarto (UNRC)-National Council of Scientific and Technical Research (CONICET), Río Cuarto 5800, Argentina
* Correspondence: cesarbarbero@gmail.com

Abstract: Direct laser interference patterning (DLIP) involves the formation of patterns of light intensity using coherent laser light beams that interfere between them. Light on the ultraviolet (<350 nm) and NIR (800–2000 nm) is absorbed in chromophores present in the polymer structure or in loaded absorbing species (dyes, polymers, nanoparticles). The absorbed light induces photothermal/photochemical processes, which alter permanently the topography of the polymer surface. The success of DLIP at different wavelengths is discussed in relation to the optical/thermal properties of the polymers and previous data on laser ablation of polymers. The size of the pattern is related directly to the wavelength of the light and inversely to the sine of the angle between beams and the refractive index of the external medium. In that way, nanometric structures (<100 nm) could be produced. Since the patterning occurs in a single short pulse (<10 ns), large surfaces can be modified. Both bacterial biofilm inhibition and human cell differentiation/orientation have been achieved. Large improvements in technological devices (e.g., thin film solar cells) using DLIP structured surfaces have also been demonstrated. Prospective application of DLIP to common polymers (e.g., Teflon[®]) and complex polymeric systems (e.g., layer-by-layer multilayers) is discussed on the basis of reported polymer data.



Citation: Barbero, C.A.; Acevedo, D.F. Manufacturing Functional Polymer Surfaces by Direct Laser Interference Patterning (DLIP): A Polymer Science View. *Nanomanufacturing* **2022**, *2*, 229–264. <https://doi.org/10.3390/nanomanufacturing2040015>

Academic Editor:
Andres Castellanos-Gomez

Received: 17 October 2022
Accepted: 21 November 2022
Published: 29 November 2022

Publisher's Note: MDPI stays neutral with regard to jurisdictional claims in published maps and institutional affiliations.



Copyright: © 2022 by the authors. Licensee MDPI, Basel, Switzerland. This article is an open access article distributed under the terms and conditions of the Creative Commons Attribution (CC BY) license (<https://creativecommons.org/licenses/by/4.0/>).

Keywords: laser; surface; polymers

1. Introduction

The manufacturing of repetitive patterns of micrometric/nanometric sizes on surfaces can be used to improve their properties, being those optical [1], of wettability [2], adhesivity [3], or cell growth [4]. Strips or dots of a material could be produced by selective removal of thin films deposited on another substrate [5]. If the underlying substrate (e.g., metal) has different surface properties from the film, the bared regions could act as a periodic array of active areas with special mass transport properties. This is the case for of ultramicroelectrode arrays [6]. Several techniques have been used to produce the patterns, including photolithography [7,8], nanosphere lithography [9], embossing [10,11], contact printing [12], and so on. They usually require several physical/chemical steps and/or expensive masks. Direct laser interference patterning (DLIP) is able to produce repetitive patterns of lines or points in one step, during a short time (<20 ns), at high repetition rates, in air, and without additional procedures [13]. The technique was developed to topographically modify a semiconductor [14]. Then, it has been applied to metals [15], ceramics [16], and polymers [17].

Two or more beams of coherent laser light interfere in the region where they superimpose, creating a sinusoidal pattern of light intensity. Low-intensity light patterns could be used to produce reactive chemical species (e.g., radicals), which initiate the polymerization chain of monomers or produce the cross-linking of prepolymers [18]. The method is called interference lithography (IL) and requires a predeposition of thin layers of the reactive monomer (or prepolymer) called resists. After the formation of the pattern, removal solvents of the monomer are required. Moreover, they usually produce cross-linked resins,

instead of linear polymers [19–21]. However, the widespread uses of photochemical 3D printing [22], which uses similar prepolymers and photoinitiators, could renew the interest in IL. On the other hand, direct laser interference patterning (DLIP) works by immediate and dry removal of the polymer from the illuminated zone (or at least the zone where the intensity is above a given threshold) in a single step. (By making a pattern in a hard surface (e.g., metal) using DLIP, it is possible to create replicas by embossing a soft material (e.g., a polymer). However, such scheme lacks the flexibility of DLIP on polymers and requires several steps.) Since short pulses (ns, ps, or fs duration) are used, the whole process can be made with a high repetition rate (e.g., 1 Hz). In that way, large areas can be modified by focusing the pattern on contiguous areas. Moreover, complex macroscopic patterns of treated areas could be made by X–Y displacement of the laser head or substrate. For example, a microfluidic device could be made where the channels are built by aligning successive spots of DLIP, which changes the wettability of the substrate, inducing liquid surface flow. The underlying phenomenon is the photoablation of polymers (due to photothermal and/or photochemical effects). While there is a large amount of information produced by polymer photoablation research, which could be of use in DLIP of polymers, it has not been extensively used. Since DLIP is more technologically oriented, it uses lower-cost solid-state lasers (e.g., Nd:YAG), while photoablation uses mainly more complex gas excimer (e.g., XeCl) lasers. One advantage of excimer lasers is the possibility to reach far UV wavelengths (e.g., 157 nm), without nonlinear doubling, with high fluences (>200 mJ/cm²). At those wavelengths, all organic materials absorb light because there are electronic transitions of single bonds ($\sigma \rightarrow \sigma^*$ and $n \rightarrow \sigma^*$). Excitation of those orbitals causes breaking of the polymer chains. On the other hand, solid-state lasers have their fundamental mode in the NIR (e.g., 1064 nm for Nd:YAG) and only reach far UV by nonlinear harmonic frequency doubling (e.g., 213 nm by using the fifth harmonic of 1064 nm), with a large decrease in achievable fluence (see below). DLIP also requires using optical elements to split and direct the beams, which have to be reflective/refractive at the wavelength of the light. This can be difficult with far UV (<200 nm) light, where even quartz is absorbing.

The application of DLIP to nonmetal materials (including polymers) has been reviewed [23] from the physics/engineering point of view. Being that polymers are organic chemical entities, a critical review of the works on the subject from the polymer chemistry point of view could help understand previous works and, more importantly, expand the use of DLIP to other polymers. For that purpose, previous successful application of DLIP to polymers is discussed, with emphasis in the properties required, such as optical absorption, thermal stability, and feasibility of photoablation. In that sense, relationships between chemical structure and successful DLIP is ascertained, together with a review of materials' available data (optical absorption spectra, thermal/photochemical stability, photoablation), which could be used to plan the application of DLIP to other polymers. Additionally, other strategies (doping with dyes, use of shorter wavelengths, use of ultrashort pulses) available for applying DLIP to new polymers will be described. Such approach seems to be required as common polymers (e.g., PDMS) used in relevant technological applications (e.g., biomedical devices) have not been structured using DLIP. In the last section, the relevant data on those polymers will be discussed.

It should be mentioned that another way to produce a pattern on polymers involves LIPSS (laser-induced periodic surface structure) [24]. LIPSS phenomena originate from the interference of the incident and reflected/refracted laser light with the scattered light close to the interface. The interference leads to surface instabilities, which develop into surface ripples. While LIPSS could alter the surface in a similar way as DLIP, it lacks the deterministic patterning capability of DLIP. Since the efficiency of the absorption/ablation process is lower for LIPSS than for DLIP, the technique has been applied to more diverse materials than DLIP [25]. On the other hand, it should be mentioned that both phenomena could occur simultaneously, creating hierarchical structures [26].

1.1. Theory of Formation of Light Patterns by Interference

Patterns of light intensity can be created by the interference of two or more light rays. Shining the pattern onto a surface (interface between a transparent and absorbing material) allows for producing physical or chemical changes in the material, which generate permanent topographic patterns. The distance between maxima (for two rays) is:

$$P = \frac{\lambda}{2n \sin(\theta/2)} \quad (1)$$

where λ is the wavelength of the laser light, n is the refractive index of the light incoming medium, and θ is the angle between the beams. (It is noteworthy that in most published works, n in the equation is omitted since the incoming medium is air ($n = 1$). The pattern of light on the surface (using two beams) shows parallel ridges with submicrometric separation (Figure 1).

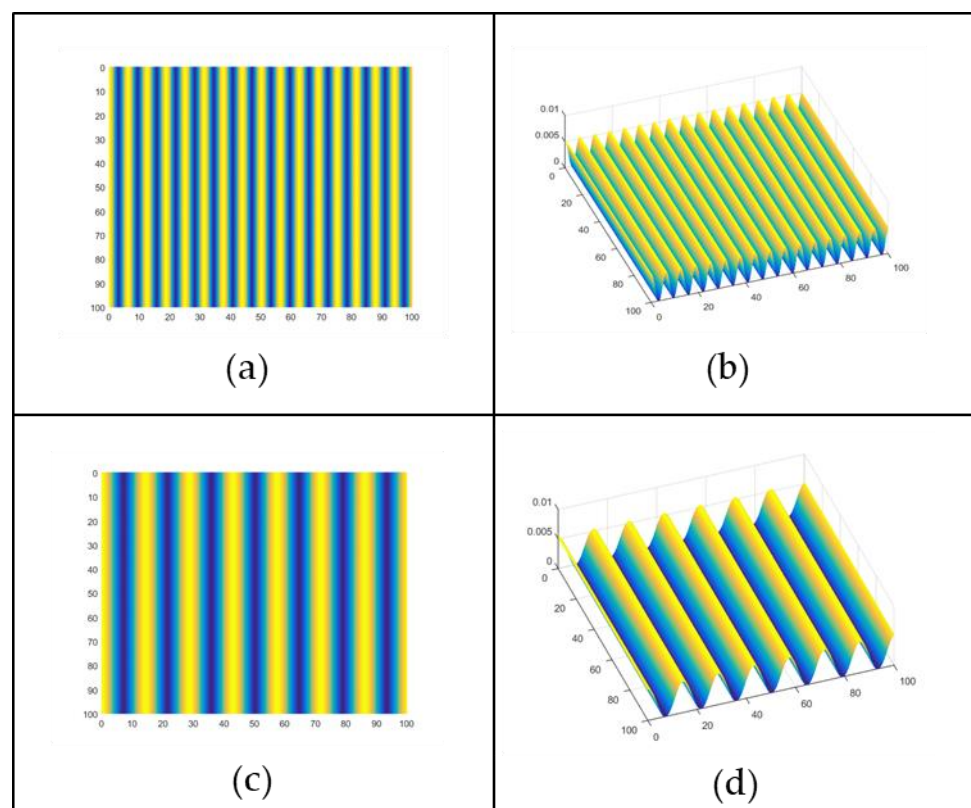


Figure 1. Pattern of light intensity produced by the interference of two beams: (a,c) top view and (b,d) 3D view. (a,b) are calculated with an angle of 67.5 degrees, while (c) is calculated with an angle of 81 degrees.

The characteristic separation and size of the structures (e.g., lines) depend on the angle between beams, the wavelength of the light, and the refractive index of the external medium (Equation (1)). The angle is the easier parameter to change.

In Figure 2 are shown the different periods of a structure that can be produced using different angles (and wavelengths). A parameter seldom changed in DLIP is the refractive index of the medium in contact with the surface. However, in Equation (1) can be seen that changing the refractive index could reduce the size of the period. Since there are transparent liquids (e.g., 1-bromonaphthalene, $n = 1.65$) or solids (e.g., quartz $n = 1.65$) with a large refractive index, the size of the period could be reduced by 55%–65%. However, to the best of our knowledge, all experiences with DLIP have used air ($n = 1$) as light incoming medium. As it can be seen in Figure 2, changing the wavelength of the laser light, the angle,

and the refractive index of the external medium, it is possible to produce structures with sizes ranging from micrometric sizes (4798 nm) to subwavelength periods (133 nm, in air, $n = 1$). The period would be in the nanorange (81 nm) using a different transparent light incoming medium (e.g., quartz, $n = 1.65$).

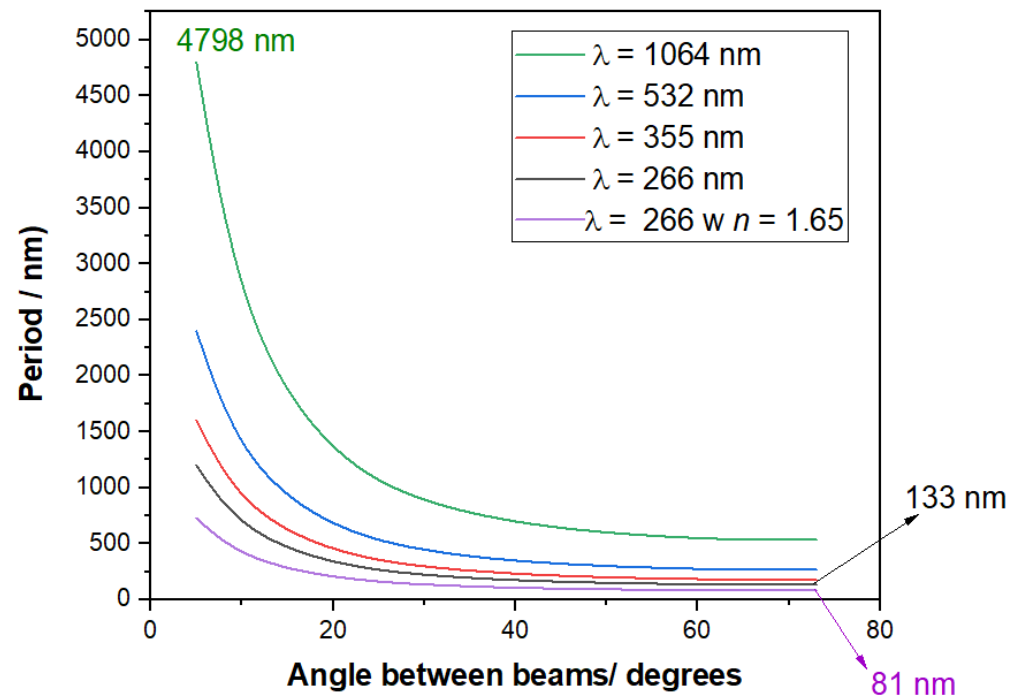


Figure 2. Effect of angle between beams, wavelength of the light, and refractive index of the external medium.

It is noteworthy that nanometric features are relevant for nanomanufacturing surfaces, but in some applications (e.g., oriented cell growth), micrometric-sized structures are required. To obtain large structures, light in the NIR range has to be used. While the angle and refractive index can be changed without affecting the light/material interaction, to produce DLIP patterns, the wavelength is usually changed to ensure the interaction of the light beam with the material. The extinction coefficient depends strongly on the wavelength of the light. In the UV–VIS–NIR range, the main absorption process in polymers is related to electronic transitions from the fundamental to the excited state of the chromophore.

Most of the DLIP structuring has been made with two interfering beams, producing periodic line patterns. However, different structures (e.g., spherical holes) can be made by DLIP using three beams (Figure 3). More complex structures can be made using four or more beams with additional experimental complexity.

The light intensity pattern translates into an array of holes on a flat surface by ablation in the illuminated regions (more precisely in the region where the light intensity is above a threshold value). The remaining material will not have a smooth appearance but contain the sharp borders of the holes and ejected polymer parts. However, polymer ablated patterns are sharper than metals, where the material only melts and remains in the borders. On the other hand, if the light does not ablate but forms gases below the surface, the polymer (softened by heating) will expand to give hemispherical shapes with a smooth finishing. Obviously, at higher overall light fluences, the bubbles could explode, and craters are created.

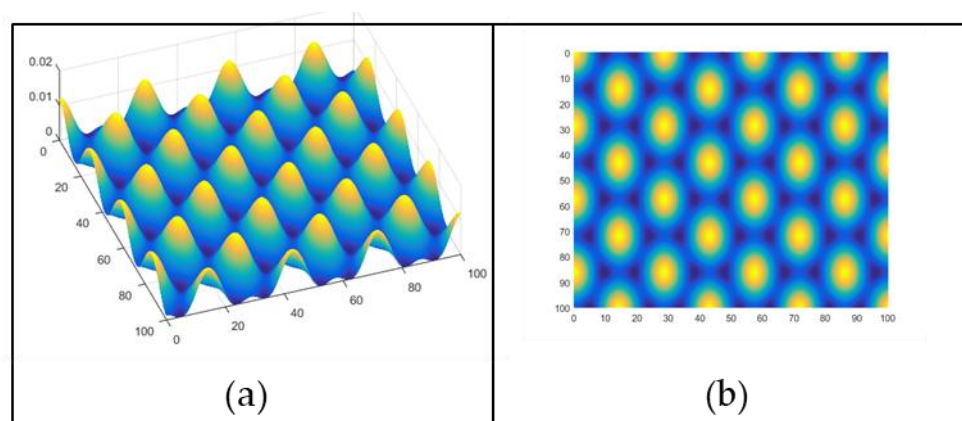


Figure 3. Pattern of light intensity produced by the interference of three beams: (a) 3 D view; (b) top view calculated with an angle between beams of 81 degrees.

1.2. Interaction of Light with Polymer Materials

To produce heat, with the forthcoming chemical and physical phenomena, the light has to be first absorbed by the chromophores (functional groups that absorb light) present in the material. In the UV–VIS range (200–800 nm), the light induces the electronic transition between the fundamental and the excited state of the chromophore. Usually, the excited electrons decay by transferring their energy to the vibrational states of the chromophore or linked groups. The vibrational energy appears as heat. The electronic transitions in the UV–VIS range are $\pi \rightarrow \pi^*$, $n \rightarrow \pi^*$, and $n \rightarrow \sigma^*$. The $\pi \rightarrow \pi^*$ transitions are “allowed” transition where a good overlap exists between the bonding and antibonding orbitals. Molar extinction coefficients (ϵ) of chromophores with $\pi \rightarrow \pi^*$ transition are above 1000. All double bonds (C=C, C=O, C=N) have $\pi \rightarrow \pi^*$ transitions, including aromatic rings. Common polymers, such as PET, PMMA, PS, PC(BPA), and PI, have groups that absorb in the UV range. Moreover, there are plenty of low-molecular-weight molecules (e.g., tartrazine) that absorb in the UV–VIS range with large ϵ . Therefore, a nonabsorbing polymer loaded (“doped”) with such dye will suffer photothermal/photochemical effects at the wavelengths where the dye absorbs.

The $n \rightarrow \pi^*$ and $n \rightarrow \sigma^*$ are “forbidden” electronic transitions with a poor overlap of the fundamental (n , nonbonded orbital) with the antibonding simple (σ^*) or double (π^*) orbitals. The molar extinction coefficient is below 1000. The $n \rightarrow \pi^*$ transition exists in double bonds with heteroatoms (C=N, C=O), while the $n \rightarrow \sigma^*$ transition occurs in simple bonds with heteroatoms (C-O, C-N, C-X (halogen)). The energy of the transitions follows the order $n-\pi^* < \pi-\pi^* < n-\sigma^*$. In the far UV range (<200 nm) occur $\sigma \rightarrow \sigma^*$ (e.g., C-C bonds) and high-energy $\pi \rightarrow \pi^*$ transitions (e.g., isolated C=C bond). Therefore, most organic materials (e.g., polypropylene) will absorb in the far UV range. However, in that wavelength range, gases in air (N_2 , O_2) also has optical absorption bands. Therefore, the whole optical setup has to be in vacuum or noble gases (e.g., He).

Extended conjugation (-C=C-C=C-, -C=C-C=O, -C=C-C=N-) creates new occupied (HOMO) and unoccupied (LUMO) electronic levels, decreasing the energy of the transition (shifting to the near UV–VIS range) and increasing the extinction coefficients (due to higher orbital overlapping). Therefore, dyes absorbing in the visible range contain several conjugated bonds (including aromatic rings). The molecules could also have groups that donate (-OR) or withdraw (e.g., -NO₂) electrons from the conjugated bonds, lowering the energy and increasing ϵ .

The initial process is photon absorption in the polymer chains or in an added dye (which can be another polymer blended with the main polymer). Most polymers (e.g., PE) do not absorb in the visible range (380–800 nm). While aliphatic chain polymers (e.g., PP) do not absorb above 200 nm, aromatic polymers (PS, PI) show electronic transition absorptions of the aromatic ring (200–280 nm). Other chromophores are the carbonyl group (PMMA, PC) and nitrile group (PAN). In Table 1 are shown the extinction coefficient for

some common polymers in the UV range. In [4], it is claimed that extinction coefficients (as a function of wavelength) of other common polymers (PTFE, PE, and PP) (in the order of 100) were also measured, but the featureless shape of the transmission loss is likely due to light dispersion, not absorption. Accordingly, tests of laser ablation of pure PE, PP, or PTFE have been unsuccessful (see below). As it can be seen, the extinction coefficients vary significantly, depending on the chromophores present.

Table 1. Absorption coefficients (α) of common polymers at the wavelengths relevant for DLIP.

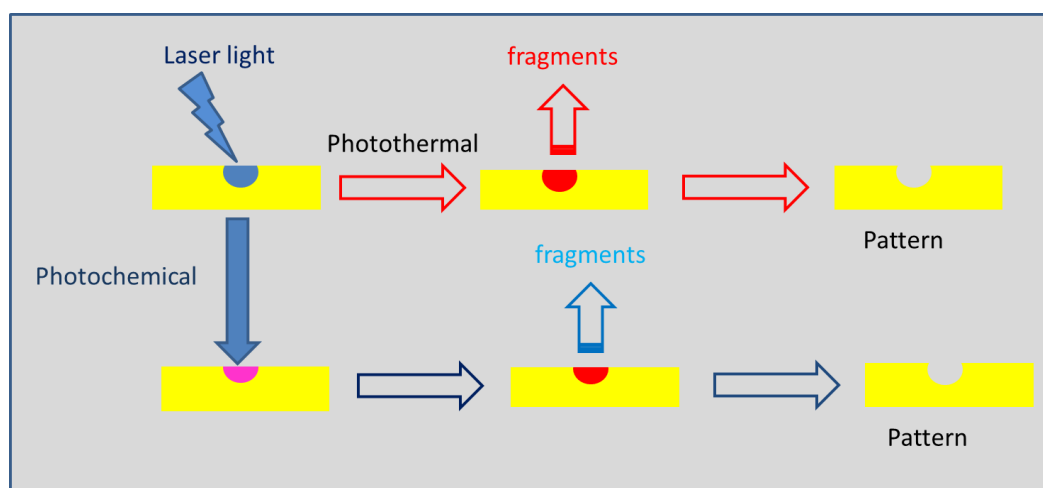
Polymer	λ_{\max} (nm)	α (cm ⁻¹)	Source
PMMA	215	6500	[27]
PMMA	250	50	[27]
PMMA	248	65	[28]
PMMA	308	<10	[27]
PVAc	215	2000	[29]
PVAc	250	100	[29]
PVAc	308	<10	[27]
PI	230	2.5 10 ⁵	[27]
PI	248	14.7 10 ⁴	[27]
PI	248	2.8 10 ⁵	[27]
PI	308	1.2 10 ⁵	[27]
PS	248	2.4 10 ⁴	[29]
P(α -MeS)	248	6.5 10 ³	[27]
P(α -MeS)	308	8.0 10 ¹	[27]
PET	250	4.9 10 ⁵	[30]
PET	308	5 10 ⁴	[27]
PEN	225	3.8 10 ⁵	[27]
PC (BPA)	248	1.0 10 ⁴	[27]
PC (BPA)	308	22	[27]
ABS	248	9.8 10 ⁴	[27]
SAN	248	7.5 10 ⁴	[29]
PE	248 and 308	<10	[27]
PP	248 and 308	<10	[27]
PTFE	248	14	[27]
PTFE	308	<10	[27]
PHEMA	222	2900	[31]
PET	308	13	[30]

In Table 1, it is specified that light absorption occurs not only at the maximum but also at other wavelengths since electronic transition bands are broad. Such behavior is relevant for DLIP because the maximum efficiency occurs at λ_{\max} but a light of closer wavelengths (e.g., 266 nm) could also have some effect and allow structuring. The light absorption of transparent polymers could be largely increased by doping with small molecules with large extinction coefficients [32]. Organic (e.g., azo) and inorganic (e.g., metal complexes) dyes could absorb strongly light (molar extinction coefficients > 10,000) and induce photoablation [33]. Moreover, the wavelength of the maximum absorption could be more easily tailored to the wavelength of the laser. Azo dyes are especially

useful for this purpose since they can be easily synthesized with λ_{\max} ranging from 300 to 600 nm. While there are plenty of azo dyes commercially available, some of them are not commercialized due to other constraints (e.g., low light fastness) and could be easily made even using combinatorial discovery methods [34]. Additionally, the azo group easily decompose thermally, producing nitrogen gas, which could expand or blow up the polymer matrix [35]. However, the material acquires coloration in the visible range and could not be used in optical applications (e.g., gratings). On the other hand, molecules that absorb in the UV (<350 nm) could be used as absorbers in DLIP when light at 266 nm (or lower) is used [36]. In that region, polynuclear aromatics (e.g., naphthalene) could be used as chromophores, with or without auxochromic groups (e.g., alkyl side chains). However, the rigidity of the extended ring system promotes radiative (fluorescence, phosphorescence) decay of the excited state. This is an energy loss for a purely photothermal mechanism but could act as a sensitizer of photochemical processes. On the other hand, polyenes have absorption maxima ranging from 180 (e.g., butadienes) to 450 nm (e.g., carotenes). The latter has the additional advantage of being a nonpolar biologically originated substance, making it ideal for structuring biodegradable polymers (e.g., PLA) since the whole dyed polymer will be biodegradable and sustainable [37].

Using another molecule as an absorber requires the homogenous dispersion in the polymer mass. Fortunately, this is also a requirement for polymer (e.g., fibers) dyeing, and a different process has been devised. The simplest one is codissolution of the dye and polymer in a solvent, followed by casting of a polymer film by solvent evaporation. Another involves coextrusion of dye containing pellets (previously dispersed in a concentrated form in the same polymer) with pellets of the pure polymer [38]. In both cases, aggregates of dye molecules should be avoided. If the material to be structured is already formed, a dissolution of the dye in a solvent mixture (solvent/antisolvent of the polymer), which swells the polymer without dissolving it, allows for coloring of the transparent polymer [39]; besides molecular dyes, absorbing polymers (e.g., PI) could also dope transparent polymers (e.g., PMMA) to induce photoablation [40]. Another way to absorb light involves ultrashort pulses (<0.5 ns), where two-photon electron absorption is possible [41].

The photoablation of the polymer in the illuminated regions (above a given intensity threshold) follows these steps (Scheme 1):



Scheme 1. Mechanism of polymer ablation due to laser illumination.

At high energies delivered, polymer chains could volatilize. Such process is nearly impossible for high-molecular-weight chains but could occur for small-molecular-weight chains, which are present in relatively low-mean-molecular-weight polymers (<100,000 g/mol) and/or in polymers with large polydispersity. The thermal energy produced in the material by the nonirradiative decay of the electronic transitions could induce thermochemical reac-

tions. Some polymers depolymerize when reaching its ceiling temperature (e.g., PMMA at 220 °C [42]); others degrade at higher T (e.g., ca. 350 °C for PI) [43]. In principle, the heat produced in the illuminated region could dissipate to the nonilluminated region. However, organic polymers are poor conductors of heat. Therefore, most of the thermal energy produced by the nonradiative transition of chromophores heat up the illuminated region and do not flow to other parts of the material [44].

The light could induce different physicochemical processes, for example, the induction of polymer chain scission by photochemical process. This is a well-known process in photolithography and does not require a large number of scission points since a decrease in the mean molecular weight of the polymer increases its solubility in some solvents (compared with the nonilluminated zones) and allows removing the affected polymer developing the image. The use of continuous laser calls for relatively large exposition times (up to seconds) and requires control of mechanical vibrations. Pulsed lasers deposit a large amount of energy (J/cm^2) on the materials during a short period of time (<10 ns), which makes unnecessary such vibration control (for single pulses). The light is absorbed by the material (or absorbing molecules incorporated into it) and increases locally the temperature. Since most polymers are poor heat conductors, the local heating could be large (>100 °C). Therefore, physical processes, such as melting, crystallization/amorphization, or even polymer sublimation, could occur. Moreover, chemical processes, such as chain scission, depolymerization, pyrolysis, or other degradation processes, could occur. In low absorbing materials, light absorption occurs in and below the surface. If gaseous (or liquid vapor) products are produced, they could be trapped inside the material and a protruding pattern could occur. Such process allows for creating complex structures with smooth surfaces. Such process occurs when light penetrates inside the material, that is, when the extinction coefficient is relatively low. On the other hand, large extinction coefficients translate into a small penetration depth. The relevant parameter is the period of the interference pattern that determines the distance between the valleys (or the crest of the ridges in expanded material). However, the size of the ablated structure depends also on how the light pattern translates into the solid pattern. The light pattern is sinusoidal (Figure 1).

If the ablation occurs at any light intensity, the solid will show an ablation pattern closely similar to the light pattern (Figure 1). However, a more common situation is ablation occurring only when light intensity surpasses a threshold value. In that case, only the higher intensity part of the pattern will be inscribed in the solid (Figure 4).

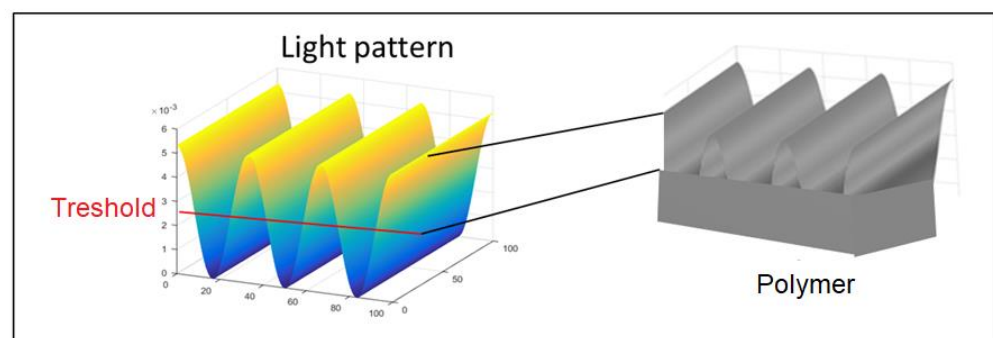


Figure 4. Transcription of an interference light pattern into a polymer pattern when the ablation occurs only at light intensities above a threshold.

Ablated regions smaller than the period of the light pattern could be produced. To achieve that, the laser intensity should be controlled, which can be performed by interposing semitransparent dispersive optical elements. Sometimes (e.g., fabrication of conductive nanostrips by the ablation of a conductive polymer film) the target structure is defined by the nonablated region. In that case, the ablated region should be maximized by using a light intensity large enough that most of the pattern is effective. In that way, nonablated regions smaller than the period of the light pattern can be produced.

The structuring depends on two different processes: light absorption/thermalization and polymer ablation. While polymers with aromatic groups (e.g., PS) absorb in the ultraviolet region (<300 nm), those with aliphatic backbones (e.g., polyacrylamide) do not absorb in the ultraviolet or visible region of the spectrum. Therefore, absorbing moieties should be incorporated. This can be performed by copolymerization with absorbing comonomers or absorption of dyes. Additionally, blending with absorbing polymers or fabrication of nanocomposites with absorbing materials (polymers, metal, and oxides) is an effective way to increase the light absorption/thermalization of the materials. The thermal energy produced by light absorption drives different processes. Some polymers (e.g., PMMA) depolymerizes since the ceiling polymerization is reached in the illuminated zones. Other polymers suffer chain scission, which can be a purely photochemical process, and the fragments are expelled from the illuminated region. It should be remembered that the light pulse induces a shockwave, which helps expel the material from the illuminate zone. While it is likely that some remaining material has suffered chain scission, with a concomitant decrease in molecular weight and increase in solubility, the post-treatment developing of the materials is seldom used.

It should be noted that light intensity at the interference maxima is a constructive sum of the intensity of the beams used. This has been elegantly demonstrated by Lasagni and coworkers [45] using DLIP to cut battery materials (Cu foil electrodes (metal absorption)). The intensity threshold could be reached at the interference maximum but not in a single beam. In fact, if several (e.g., 10) beams are combined, the change can be quite large (an order of magnitude). Moreover, each light beam would contain only 1/10th of the fluence at the maxima. Therefore, it could travel in an angle through a sensitive medium (e.g., biological tissue) without causing damage, but large effective fluence would be produced in the target surface. By shifting the spot (or even wobbling it), the whole surface area could be illuminated with higher fluence.

In the illuminated regions, the main phenomenon occurring is photothermal ablation (PhAb) of polymers. However, the laser light used in PhAb and DLIP is usually different. Excimer gas lasers (e.g., XeCl), in their fundamental mode in the UV, are commonly used in PhAb. On the other hand, Nd:YAG, doubled, tripled, or quadrupled, is used in DLIP. Therefore, a quite low wavelength (down to 157 nm) is used in PhAb, while 355 and 266 nm laser light is usually used in DLIP. Since several common polymers (e.g., PE) do not absorb at wavelengths above 200–250 nm, it is possible to apply PhAb but not DLIP.

Special polymers (e.g., triazene) with high light absorption and low decomposition energy threshold have been synthesized and photothermally ablated with great success [46]. The triazene group is a typical photothermophore with high optical absorption and low thermal stability [46]. Those materials could be easily structured using DLIP. Moreover, good PhAb properties relate to low thermal/chemical stability. This is a problem when the polymer negative image constitutes a resist for harsh etching procedures (e.g., oxidation), but it is not a problem in nanostructuring by DLIP of the final surface. It should be mentioned that, while effective ablation is necessary for DLIP, explosive decomposition (e.g., by release of N₂ from triazene groups) could produce ablation of the whole surface, destroying the structure. Such undesirable effects could be avoided by reducing the light fluence.

Any high-power laser light could be used. The most commonly used are Nd:YAG solid-state lasers with a pulse width of 3–50 ns and a repetition rate of 1–10 Hz. The energy of such lasers is in the range of 0.5–2 J. The wavelength of light (fundamental mode) is 1064 nm, which is in the near-infrared range. While some polymers (e.g., doped conducting polymers) absorb in that wavelength range, most polymers (e.g., PS) only absorb in the UV region. The period of the structures is proportional to the wavelength of the light (Equation (1)). Therefore, nonlinear frequency doubling is used to decrease the wavelength (to 532, 355, and 266 nm in the case of Nd:YAG). The frequency doubling is usually used to decrease the size of the features or to reach wavelength regions where light absorption occurs. In principle, photons of lower wavelength are of higher energy. The wavelength

of the laser light can be changed using nonlinear crystals, which amplify the intensity of the harmonics of the fundamental emission. For a Nd:YAG laser, the fundamental is at 1064 nm, with the first, second, third, and fourth harmonics at 532, 355, 266, and 213 nm. The energy of the photon increases with the decrease in the light wavelength:

$$E = h \frac{c}{\lambda} \quad (2)$$

where h is Planck's constant and c is the light speed in vacuum.

Therefore, it seems that decreasing the wavelength increases the energy used for DLIP. However, the nonlinear crystals have less than 100% efficiency [47]. In Figure 3, the effective energy for a commercial Nd:YAG laser and frequency doubling crystals is shown [48]. In Figure 5 are shown the raw energy of a mol of photons and the effective energy.

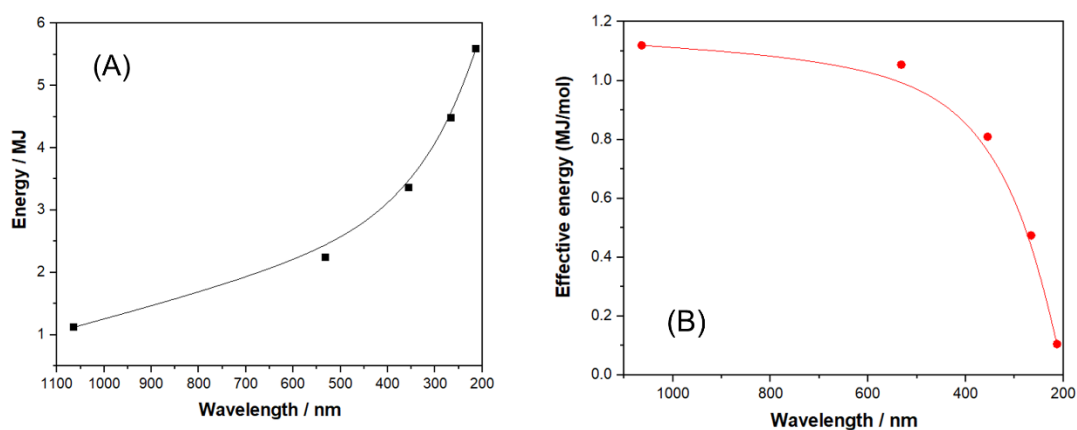


Figure 5. Energy of the laser (Equation (2)) (A) and effective energy after frequency doubling (B).

Therefore, frequency doubling is not a suitable strategy to increase the energy of the laser beam.

Since almost every organic polymer absorbs below 200 nm, DLIP using gas-rare gas excimer lasers (e.g., 157 nm) would be able to structure any polymer. However, light below 200 nm is absorbed by oxygen, and the whole setup should be purged with N_2 [49]. Moreover, DLIP requires beam splitters, and mirrors and quartz (the usual transparent material used in UV) absorb below ca. 180 nm [50]. While other materials exist (e.g., CaF_2 [51]), it is more complex to produce optical elements with those materials.

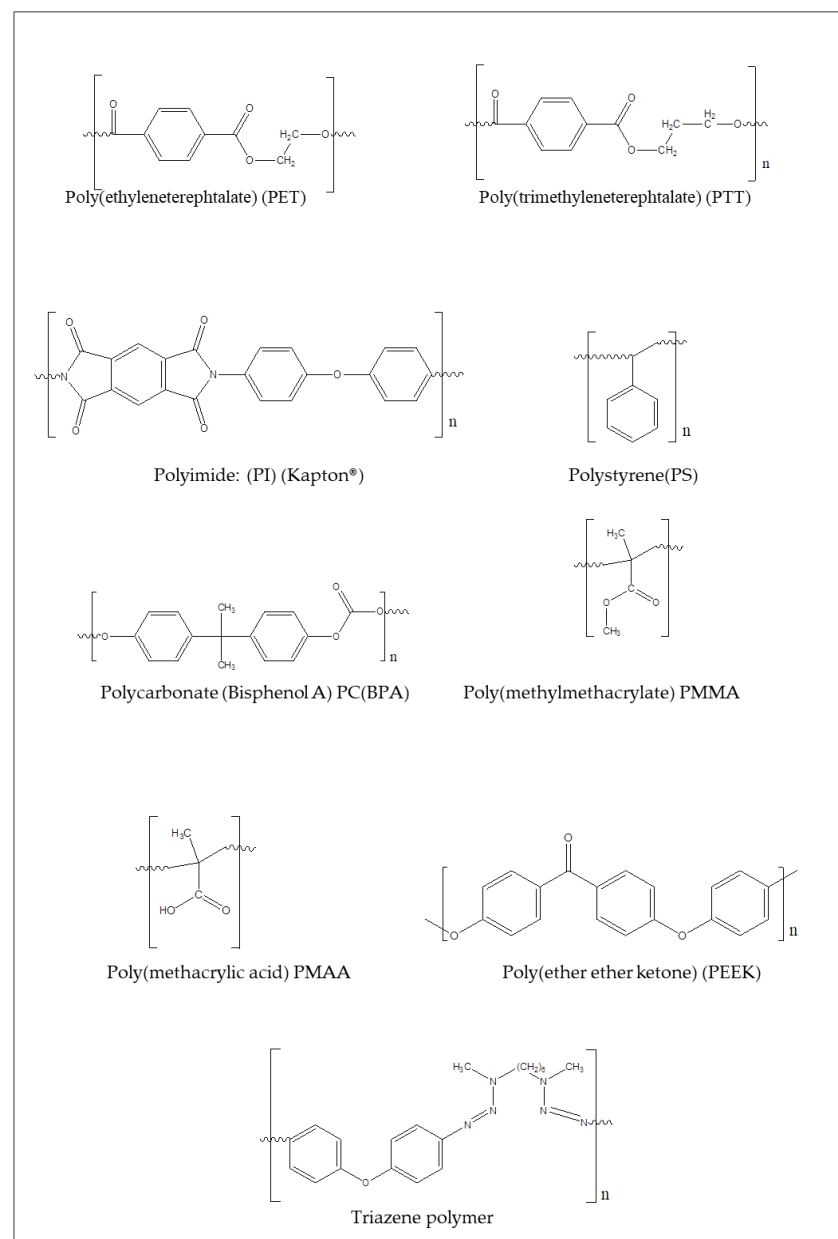
2. Direct Laser Interference Patterning (DLIP) of Polymer Materials

Polymers are macromolecules of large mean molecular weight (>10,000 g/mol). The materials do not sublime below their decomposition temperature. On the other hand, as organic materials, they usually decompose at relatively low temperatures (<300 °C). Therefore, the energy/power required to structure these materials is quite low, compared with ceramics or metals. This allows for structuring with single pulses and defocusing the laser beam on large areas (mm^2 to cm^2). In that way, nanostructuring of large surfaces is possible. On the other hand, most commonly used polymers (e.g., polyethylene) do not absorb light in the UV–VIS range of the spectrum. Therefore, absorbing moieties has to be incorporated. This can be performed by copolymerization of the main monomer with an absorbing one, or by doping the polymer with small colored molecules. Copolymerization changes not only the light absorption properties but also the thermal stability of the chains. Therefore, even a small amount of different monomer units could influence the DLIP process. The most common kind of polymers are homopolymers, that is, chains containing only one monomer unit.

2.1. Homopolymers

Homopolymers are materials containing only one monomer unit. In the case of a polymer (e.g., polystyrene) made by chain polymerization (including ring opening), the monomer unit corresponds to the actual monomer (e.g., styrene). In the case of step-growth polymers (e.g., poly(ethyleneterephthalate), PET), the monomer unit contains moieties from two reactants (ethylene glycol + terephthalic acid). However, such material is considered a homopolymer. Special cases are the polyurethanes, which are made with two or more reactants—a di-isocyanate and several diols—and are considered copolymers. The absorption of light and thermal stability is related to the structure on such monomer unit (Table 2).

The chemical structure of the monomer units where DLIP has been successfully applied is shown in Scheme 2. Subsequently, work on common polymers is described with emphasis on the relationship between the polymer chemical structure and DLIP structuring.



Scheme 2. Chemical structure of the monomer units of homopolymers structured by DLIP.

Table 2. Summary of parameters used during DLIP application to homopolymers.

Polymer	Laser	λ (nm)	Max Fluence (mJ/cm ²)	Pulse Duration (ns)/nr	Setup	Refs.	Application
PET, PI	KrF	248	200	25/mul	Michelson interferometer	[17]	Optical gratings
PI	KrF	248	58	-/mul	Talbot interferometer	[52,53]	Semiconductor processing
PI	ArF	193	300	-/mul	Talbot interferometer	[54]	Optical gratings
Triazene polymer &	Nd:YAG	355	240	1–10	Michelson interferometer	[55]	Optical gratings
PC	KrF	248	-	0.5/single	Diffraction variable delay generator	[56]	Photonic crystals
PET @	Nd:YAG	266	500	10/1–10	MMI *	[57,58]	Biological cell adhesion/growth
PET	Nd:YAG	266	20–400	10/1	MMI	[59]	Solar cell
PET	Nd:YAG	266	100–150	10/1	MMI	[60]	Optical gratings
PET	Nd:YAG	266	20–400	10/1	Diffraction	[61]	Optical gratings
PI, PS	Nd:YAG	266&355	500	10/1	MMI	[62]	Inhibition biofilm
PI	fs	1030	0.5	<0.5/5–10	Diffraction	[63]	DLIP + LIPSS
PI	Nd:YAG	355	-	10/1	MMI	[64]	Antifouling/antibacterial
PS	Nd:YAG	266	500	10/1	MMI	[65]	functionalization of surfaces
PS, PI, PET	Nd:YAG	266	500	10/1	MMI	[66]	Bacterial anti-biofouling
PS	ps	1064	0.001	$10 \times 10^{-3}/1$	DOE	[67]	Surface patterning
PTT	Nd:YAG	266	-	10/1	MMI	[68]	Proof of concept
PC	Nd:YAG	266	>300	10/1	MMI	[69]	SERS
PC, C@PC	DPSS	263	0.05	3/1	DOE	[70,71]	Modelling
PC	Nd:YAG	355	0.05	0.01/1	DOE	[26]	Micromachining
	Nd:YAG	266	180	<10/1	DOE		
	DPSS	263	0.05	<3/1	DOE		
PC	DPSS	263	0.05	3/1	DOE (DLIP)	[55]	Hierarchical micro-/nanostructures
	Yb:YAG	343	2–4	0.007/1000	1 beam (LIPSS)		
	Nd:VAN	355	2–4	0.010/1000	1 beam (LIPSS)		
PC	KrF	248	-	<0.0001/1	DVDG	[72]	Photonic crystals
PMMA, PS, P(MMA-co-S), PI, PC	Nd:YAG	266 355	300	10/1	MMI	[72]	Effect of polymer and fluence
Doped PS	Nd:YAG	266 355	300	10/1	MMI	[73]	Cell growth
PI, PEEK	Nd:YAG	355	1.2	38/1	MMI	[74]	Embossing of PDMS for guiding neurons
PMMA with Ag Nc	Nd:YAG	355	800	6/1	MMI	[75]	Fluorescent patterning

Table 2. Cont.

Polymer	Laser	λ (nm)	Max Fluence (mJ/cm ²)	Pulse Duration (ns)/nr	Setup	Refs.	Application
PEEK-CF composite	DPSS	1053 263	1.4, 2.9 2	15/1 4/1	DOE	[76]	Superhydrophobic surfaces

@ Thermanox[®] with proprietary additive. * Modified Michelson interferometer. & Custom-made polymer [77].

2.1.1. Poly(ethyleneterephthalate) (PET) and Related Polyesters

PET has an aromatic (terephthalic) ring in the polymer chain (Scheme 2), which absorbs in the far UV. In fact, a similar phthalate ester (ethyl dibutylphthalate) shows a molar extinction coefficient of ca. 12,000 at 303 nm [78]. Moreover, PET begins to thermally degrade, with the formation of volatile products, at 280 °C [79]. PET photoablation was demonstrated [80]. Ilcisin and Fedosejevs, described the first application of polymer ablation using interference (what they called holographic diffraction) to produce optical gratings in PET and PI films [17]. The setup to produce the interference was similar to a Michelson interferometer. They produced gratings with periods between 250 and 1259 nm, where the produced structure period agreed with the light pattern within the measurement error (2%). They also tried manufacturing grating with PE, PTFE, and PMMA without success, likely due to the weak absorption of those polymers at 248 nm. Yu et al. studied the structuring of a modified PET (Thermanox[®]) [57]. The PET films were treated by the commercial producer to improve cell adhesion and growth with a proprietary procedure. The effect of laser fluence and angle on the patterns was thoroughly studied using AFM, XPS, and ATR-FTIR. In a related study, the patterned Thermanox[®] films were coated with collagen, and biological cell was grown on them [57]. The period of the grooves created on the PET film was between 1.2 to 9.7 μm . At a small period, the cells (mouse fibroblast) oriented parallel to the axis of the grooves. On the other hand, on large grooves, the fibroblast oriented randomly with respect to the axis. Klein-Wiele and Simon used a diffractive element (DVDG) as a generator of an interference light pattern to structure PC with a high fidelity of the polymer surface pattern with the light pattern [69]. Müller-Meskamp et al. structured transparent PET films at 266 nm to be used as a patterned substrate of thin film organic solar cells [59]. The controlled structuring increased the efficiency of light collection and energy production. Perez-Hernandez et al. manufactured optical gratings on PET using DLIP (266 nm) [60]. The best diffraction efficiencies were measured in gratings fabricated with one laser pulse at low fluences (100–150 mJ/cm²). In that way, fast manufacturing (up to 18 cm²/s) of diffraction gratings was demonstrated. In a further publication of Lasagni and coworkers, a complete modeling of the DLIP process on PET allowed for improving the diffraction efficiencies and for implementing the permanent patterns as holographic tags against counterfeiting [61]. Recently, Martin-Fabiani et al. used DLIP to structure another polyester: poly(trimethyleneterephthalate) (PTT) [68]. The monomer unit of PTT contains one additional methylene (-CH₂-), compared with PET, in the diol part (Scheme 2). However, while rotation along the single C-C bond in PET is sterically impeded, both C-C bonds in PTT could rotate, making a more flexible chain. This chemical structure affects the physical properties of the polymer. PTT shows a T_g of 44–60 °C and a T_m of 220–231 °C compared with T_g = 67–81 °C and T_m = 256–267 °C for PET [81]). Such differences could affect the melting of the polymer upon irradiation. However, the acid residue in both polymers is the same (terephthalic acid). Since the aromatic ring is the chromophore in PET, the optical properties should be similar. Indeed, the extinction coefficient is $2.6 \times 10^5 \text{ cm}^{-1}$ (at 266 nm), quite similar to that of PET (4.5×10^5 at 250 nm, Table 1). The authors reported micrometric and submicrometric patterns on PTT. Using a complete Gaussian profile of the laser spot (instead of a top-hat filtered profile) allows for seeing the effect of different fluences on the same sample. In that way, complete ablation is observed at the center of the spot and just polymer melting at the edges. PET is one of the

most widely used polymers. Since it could be chemically recycled to form virgin polymer, it could be used in a sustainable way. However, there is a growing use of bio-based polyesters, such as poly(alkylenefuranoates) [82]. In those polymers, the only chromophore will be the ester group, giving optical properties similar to those of PMMA.

2.1.2. Polyimide (PI)

The name polyimide (PI) denotes a whole class of polymers having the imide group in the monomer unit [83]. The one usually used in DLIP work is Kapton[®], which is the poly(4,4'-oxydiphenylene-pyromellitimide). As it can be seen, there are three aromatic rings per monomer unit (Scheme 2), which could act as chromophores for light absorption in the UV. The UV–VIS spectrum of PI films shows a large band in the UV with shoulders (decreasing absorption) at 218, 276, 334, and 378 nm. In fact, Kapton films are strongly colored (orange-brown), suggesting some optical absorption in the visible region (>380 nm). Model compounds of the PI monomer unit has a large absorption in the K band of the aromatic ring with shoulders (of decreasing absorption at 310, 328, and 371 nm) [83]. Resonance Raman spectroscopy allows for assigning the intense $\pi \rightarrow \pi^*$ transition of the central phenyl group at 300–330 nm and a weaker R band ($n \rightarrow \pi^*$) at a lower frequency, which red-shifts and intensifies to a K band ($\pi \rightarrow \pi^*$) upon conjugation related to the aromatic substitution at the N atom [83]. The absorption bands of PI allows for photoablating PI with different laser lines, including 248 (KrF excimer), 266, and 355 nm (frequency-doubled Nd:YAG) [84]. On the other hand, PI is quite thermally stable, with pronounced degradation only at 550–580 °C [84]. Photoablation of PI using both UV (248 nm) and NIR (>1040 nm) laser light was demonstrated [85]. Besides the photothermal mechanism, photochemical degradation could also occur [86]. As it is shown in Table 1, PI (Kapton) was structured in the same conditions as PET to form optical gratings [17]. Since PI (Kapton) shows strong coloration (orange-red), it is only suitable for reflective gratings, after coating the patterned polymer with a metal (e.g., Al). On the other hand, it could be used for nonoptical applications. Günther et al. manufactured patterned surfaces of PI by DLIP (355 nm) to control the formation of biofilms by *Staphylococcus epidermidis* [26]. Using two- and three-beam configurations, patterns of lines, pillars, and lamella were produced. The in vitro growth of bacteria on the surfaces was compared with the nonpatterned substrate. The efficiency of biofilm formation followed the trend lines > pillars > lamella > flat surface. Moreover, the surface patterned as lamella showed the least biofilm formation in in vivo studies. Alamri et al. used a femtosecond (1030 nm) laser to structure surfaces of PI [63]. DLIP patterns were present together with LIPSS patterns. In that way, hierarchical (micrometric sized by DLIP and nanometric sized by LIPSS) features were produced. It was assumed that two-photon absorption occurs with the ultrashort (fs) laser since PI does not have an electronic transition at 1030 nm. However, two-photon absorption will shift the light to double the energy (515 nm), where PI still does not show optical absorption [63]. Moreover, it has been shown that continuous IR light (CO₂ laser) could photoablate PI [86]. In the NIR region (>800 nm), there were no electronic transitions (in dielectric undoped polymers), but existed the harmonics of the vibrational bands (e.g., C-H) present in the functional groups. In the region of 1000–1100 nm, there was absorption of the third harmonic of the C-H stretching in aromatic rings [87]. Such an effect has been shown to be responsible for the photoablation of poly(ethyleneglycol) with an infrared laser [88]. Cuello et al. manufactured patterned (arrays of grooves with periods of 1, 2, and 10 μm) surfaces of PI to control bacterial (*Pseudomonas aeruginosa*) growth [64]. The DLIP structuring changes the roughness of the surface (Table 3). The roughness correlates with an increase in the contact angle of water (Table 3), as expected for the existence of Cassie-Baxter effects [89]. The lower surface of the water drop interacts only with the top of the polymer structures. Water does not penetrate the trenches due to the high surface tension. Therefore, the millimeter-sized drop interacts with an effective medium surface made of air (hydrophobic) and polymer. In that way, the surface shows a more hydrophobic nature than the flat polymer surface. The change in wettability induces a large antifouling effect, where a large decrease (>90 %) in

bacterial cell growth is observed for all structured surfaces. The micrometer-sized cells also sit on top of the polymer structure. Interestingly, the effect observed for the same base polymer (PI) with *Pseudomonas aeruginosa* (Gram negative) is quite different from that observed for *Staphylococcus* spp. (Gram positive) [26]. Since the Gram dyeing test is related to the chemical nature of the bacterial walls, it is reasonable that the interaction with the surfaces is different.

Table 3. Effect of DLIP structuring of a PI surface on the growth of bacterial cells.

Period (μm)	Contact Angle/ $^\circ$	Roughness (nm)	Cells per mL $\times 10^{-7}$
0 (flat)	65	1.4	49.5
1	101	33.4	4.3
2	92	28.9	2.76
10	72	19.4	5.88

Bremus-Koebberling et al. manufactured line arrays in PI to emboss PDMS and create surfaces able to orient neuronal cell growth [74].

2.1.3. Polystyrene (PS)

PS has a chain with aromatic (alkyl-substituted) rings (Scheme 2), which shows broad absorption bands in the UV region (260 and 290 nm (shoulder)) in solution. The band at 260 nm is assigned to the K ($\pi \rightarrow \pi^*$) band of the aromatic ring. The shoulder (290 nm) is assigned to a charge transfer band between neighboring rings [90]. From the spectrum, it can be predicted that PS can be structured with 266 nm laser light but not with 355 nm. Such results are observed experimentally. TGA measurements of pure PS show weight loss beginning at 215 °C [91], indicating low thermal stability. Indeed, PS films have been photoablated with light at 248 nm (KrF excimer laser) [92]. Guenther et al. manufactured patterned surfaces of PS by DLIP (266 nm) to control the formation of biofilms by *Staphylococcus aureus* [26]. Using two- and three-beam configuration, patterns of lines and pillars were produced. The bacteria formed a biofilm on the surfaces with efficiency lines > pillars > lamella > flat surface. The surface patterned as lamella showed the least formation in in vivo studies. It is noteworthy that PI (the other polymer structured in this work [26]) is polar/hydrophilic while PS is clearly hydrophobic. However, the trend on the bacterial growth of the structuring is the same. Valle et al. manufactured patterned surfaces of PS, PI, and PET by DLIP and tested the growth of *Staphylococcus aureus* [66]. The results suggest that ridge or pillar structures promote the growth while lamella-like structures strongly inhibit the formation of a biofilm. The use of high-repetition lasers allows for applying DLIP in massive scales. Ränke et al. used a picosecond laser with a DOE optical element [67]. Scanning the spot on the surface allows for structuring PS at a rate of 1.1 m²/min. Like in the case of PI [26], an ultrashort pulse laser is used to structure a polymer (PS) at a wavelength (1064 nm) where no electronic transition exists in the chromophores of the chains [93]. Two-photon absorption will shift the absorption to 532 nm, where PS is completely transparent. However, a large concentration (5 per monomer unit) of aromatic C-H groups is present where the third harmonic of the vibrational band (C-H stretching) is in the 1000–1100 nm regions. Doping of polymers involves the incorporation of molecules, including macromolecules, which absorb light at a given wavelength where the polymer is transparent, which is a well-known technique to allow polymer photoablation [94]. Besides optical absorption, the doping agent could also decompose producing gaseous products (e.g., N₂), which remove the polymer matrix in the illuminated region [94].

Brogia et al. generated line-like periodic patterns by DLIP on doped PS (d-PS) using light at 355 nm (where PS has no intrinsic absorption) [73]. An azo dye (2-anisidine \rightarrow 2-anisidine) is codeposited with PS from chloroform solution. DLIP on d-PS results in the swelling of the surface at low fluences and ablation at high intensities. The results are

similar to single-beam irradiation of doped PMMA [95] and contrast with the usual process of DLIP on PS where only ablation is detected. It seems that decomposition of the azo dye (with release of N₂) is the driving force of the expansion. The data from in vitro assays show that fibroblast cells are attached and proliferate extensively on structured d-PS [74].

2.1.4. Polycarbonate (PC)

Polycarbonate is the name of a family of polymers that are made of diesters (with diols) of the bifunctional carbonic acid. It is possible to produce polycarbonates of every diol (diphenol or dialcohol), but the most common commercial one (used with DLIP) contains bisphenol A as a diol unit (Scheme 2). Such caveat is important because the aromatic rings in the bisphenol A unit are the light absorbing center (allowed K ($\pi \rightarrow \pi^*$) transitions of the aromatic ring (265 and 275 nm) with $\epsilon > 10,000$) [96]. A polycarbonate with aliphatic diol units (e.g., poly(propylenecarbonate) [97]) absorbs only weakly due to transitions in the $>C=O$ group (“allowed” $\pi \rightarrow \pi^*$ and “forbidden” $n \rightarrow \pi^*$ transition). PC is quite stable thermally, beginning its degradation at 550 °C [98]. PC(BPA) has been successfully photoablated with laser light at 308 nm (XeCl excimer laser) [99].

Acevedo et al. used DLIP to sub-micrometrically structure PC films with the purpose of building SERS-active surfaces [68]. Raman signal, measured with a continuous laser light (e.g., He-Ne at 632.8 nm), is markedly enhanced (2–5 orders of magnitude) when the analyzed molecules are adsorbed onto metal surfaces with structures sized in the order of the probing laser light [100]. The structured surfaces, made by DLIP of PC, were covered (by sputtering) with metallic (Au or Pt) thin (500 nm) films. Using different beam configurations and/or rotating the sample 90° between pulses, nonsmooth structures were produced. Those structures with smaller protruding features show more enhancement of the signal of an adsorbed organic molecule (2-thioaniline) [101]. The method has been patented (see at the end). Alamri and Lasagni patterned transparent PC films (LEXAN[®]) with DLIP (266 nm) [69,70]. A complete model structuring is proposed, which includes two types of ablation and two types of swelling. Gunther et al. used three types of different lasers on PC integrated with a 3D printer of thermoplastics to test the ability of using DLIP as a micromachining tool [71]. Line-like structures (period 0.7 to 10 mm) were produced. While smooth sinusoidal structures were made at low fluences (0.1–0.8 J/cm²), strong material melting induced the formation of superstructures at high fluences (>0.8 J/cm²). Mezera et al. combined DLIP with LIPSS to produce hierarchical structures with micrometric (DLIP) and nanometric (LIPSS) features [26]. When the linear laser polarization (ps laser one beam) was set perpendicular to the DLIP-formed (ns laser two beams) linear ridges, LIPSS could be formed on top of the ridges. It should be mentioned that aromatic polycarbonates face a growing environmental concern due to the role of bisphenol as an endocrine disruptor [102]. Therefore, aliphatic polycarbonates are likely to be of increased use [103]. In those materials, only the weakly absorbing carbonate (ester) group will remain as a chromophore, and it is likely for the feasibility of photoablation (and DLIP) to be affected. A way to allow DLIP of aliphatic PC involves doping with dyes (e.g., azoic), polynuclear aromatics (e.g., anthracene), or absorbing polymers (e.g., PI).

2.1.5. Polymethylmethacrylate (PMMA) and Related Acrylates

PMMA is the most widely used transparent polymer [104]. The chemical structure of the monomer unit (Scheme 2) shows only an aliphatic ester group with a $>C=O$ as chromophore. It shows two absorption bands [105], in UV due to the $\pi \rightarrow \pi^*$ (220 nm, strong) and $n \rightarrow \pi^*$ (295 nm, weak) transitions of the $>C=O$ group. PMMA degrades thermally at temperatures higher than 300 °C [106], with depolymerization. PMMA has been photoablated at 193 and 248 nm, and the formation of the monomer (MMA) by depolymerization was found to be larger at 193 than at 248 nm [107]. It is likely that not only photothermal ablation occurs but also photochemical processes occur [108]. Acevedo et al. studied the patterning of PMMA using DLIP (266 nm) [72]. The surface is ablated, but distorted shapes are produced, unlike PS, which produces smooth parallel ridges. The

monomer (MMA), produced during depolymerization, is a good solvent of PMMA and could swell/dissolve the unaffected PMMA region, blurring the shape of the structures. Mulko et al. doped PMAA with Ag clusters and used DLIP (355 nm) to create ablated structures [75]. Pure PMAA has only the carboxylic acid (-COOH) as chromophore and, like PMMA, could not be structured by irradiation at 355 nm. The silver nanoclusters, formed by irradiation with a UV lamp at 365 nm, show a broad band centered at 505 nm. Therefore, they absorb the light at 355 nm and promote polymer ablation at the illuminated regions with surface patterning. On the other hand, irradiation of a PMAA film with only retained Ag⁺ ions induces the formation of fluorescent silver nanoclusters, followed by surface patterning. The films show fluorescence (600 nm when illuminated at 488 nm), and the luminescence surface pattern follows the topographic structure. This work shows clearly the usefulness of nanoparticles as light absorbers in DLIP. If the precursor species (Ag⁺) in this case could be loaded inside a transparent material, the nanoparticles could be synthesized in situ by photochemical reactions [109]. In that way, DLIP of preformed transparent polymers or gels could be performed.

2.1.6. Poly(etheretherketone) (PEEK)

PEEK is a semicrystalline thermoplastic with excellent mechanical and chemical resistance properties, useful for biomedical applications [110]. The chemical structure (Scheme 2) contains three aromatic rings per monomer unit and a carbonyl group conjugated to two rings (benzophenone). Moreover, it contains two aromatic ether groups, which act as auxochromes. Accordingly, PEEK absorbs strongly below 410 nm [111]. On the other hand, it is thermally stable, decomposing only at 575 °C [112]. Since PEEK is easily photoablated at 308 nm [113], it is likely that a photochemical mechanism of ablation is operative. Bremus-Koebberling et al. manufactured line arrays in PEEK to use the pattern to emboss PDMS and create traces of patterned spots able to orient neuronal cell growth [74]. The rigidity of PEEK makes it an excellent mold to produce PDMS patterns. On the other hand, they found out that PDMS surfaces cannot be directly structured by DLIP. Hauschwitz et al. used DLIP (1053 and 263 nm) to structure a composite material made of oriented carbon fibers in a PEEK matrix [76]. Structuring is observed at both wavelengths, but in NIR, the C fibers seem to heat and vaporize/decompose PEEK. At 263 nm, PEEK is ablated efficiently, leaving a pattern with the fibers protruding. Using different fluences and pretreatments, it is possible to produce hierarchical structures. The inhomogeneity of the patterned surfaces, with micrometric PEEK (polar hydrophilic) and C fiber (hydrophobic) domains, makes it less hydrophobic. However, covering the whole structured surface with a fluorinated silane, superhydrophobic stable surfaces (contact angles > 170°) could be obtained.

2.1.7. Triazene Polymer

This is a specially synthesized polymer that contains the triazene group (-N=N-N-), which has large absorption in the UV and visible region [46], and decomposes thermally to give N₂. The physical and chemical stability is worse than common polymers, and its use is restricted to method development. Molecular triazenes have been used as dopants of transparent polymers [114]. Lippert et al. used interference ablation (355 nm) of a triazene polymer to produce gratings [54]. The groove spacing (180–1090 nm) can be varied with the angle between beams, while the depth is related to the laser fluence. The excellent photoablation properties of the designed polymer imply that one pulse is required to produce the gratings and additional pulses only deteriorate its quality.

2.2. Copolymers

Copolymers are materials that contain two (or more) monomer units covalently linked to the polymer chains [115]. Each comonomer adds specific properties, and the interaction between them produces materials with improved properties [116].

If one homopolymer (e.g., PMMA) could not be structured by DLIP because it has not enough light absorption at the laser wavelength light (e.g., 355 nm), it is possible to

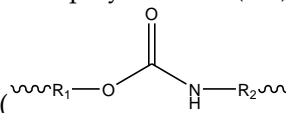
copolymerize the monomer (e.g., methylmethacrylate) with another group having larger optical absorption (e.g., vinylphenol). Since the comonomer unit is part of the main chain, its thermal degradation produces copolymer ablation. Therefore, inclusion of comonomers with a lower degradation temperature (e.g., acrylonitrile) could favor photoablation. While the same could be performed by mixing (blending) both homopolymers, most polymers are not miscible between them due to low entropic change upon mixing. On the other hand, a small amount of the absorbing polymer could be enough to allow DLIP structuring of the polymer matrix (Table 4).

Table 4. Summary of parameters used in DLIP with copolymers.

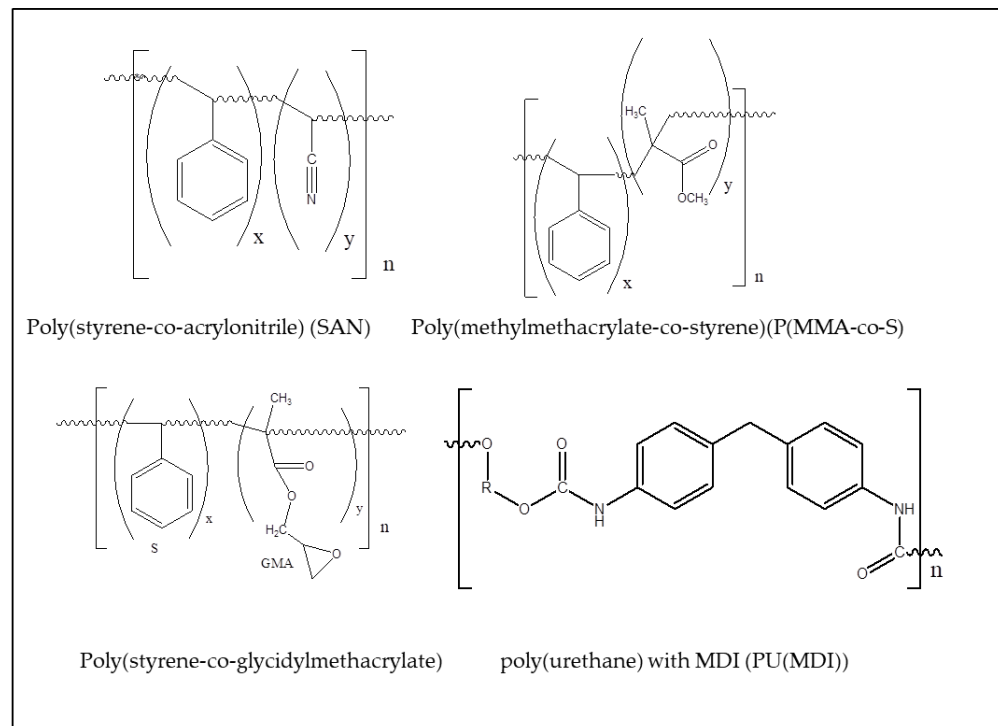
Copolymer	Laser	λ (nm)	Fluence (mJ/cm ²)	Pulse Duration (ns/nr)	Setup	Refs.	Application
PU	Nd:YAG	266	100–600	10/1	MMI	[117]	Wettability control
SAN (p(S-co-AN))	Nd:YAG	266	500	10/1	MMI	[118]	Chemically patterned surfaces
p(MMA-co-S)	Nd:YAG	266	500	10/1	MMI	[73]	Structuring PMMA
P(S-co-EGMA)	Nd:YAG	266	500	10/1	MMI	[64]	Chemical pattern reactivity

2.2.1. Polyurethane

The name polyurethane (PU) denotes a whole class of compounds, having urethane

moieties () [119]. Changing the groups linked to the urethane (R_1 , R_2), it is possible to produce materials with a variety of properties, from flexible foams, to tough engineering thermoplastics [120]. The structuring of the surface is relevant for the extensive application of polyurethanes in biomedical devices [121].

While the carbonyl group could show weak absorptions due to the $\pi \rightarrow \pi^*$ and $n \rightarrow \pi^*$ electronic transitions, the main absorption would exist if any of the groups (R_1 , R_2) linked to the urethane moiety contains an aromatic ring. In fact, polyurethanes are alternating copolymers since they contain a rigid R_1 group (usually an aromatic ring from a diisocyanate) and a flexible R_2 group (usually alkyl chains from diols). Polyurethanes are usually made by reacting (step-growth polymerization) a diisocyanate with a diol. A common diisocyanate is MDI (methylene diphenyldiisocyanate) (Scheme 3). An MDI based PU has a broad absorption band at 293 nm [122]. It should be noted that industrial MDI includes also the 2,2'- and 2,4'-isomers and could include polymeric forms. However, the chromophores present (methylene- and urethane-substituted aromatic rings) are similar, leading to similar optical properties. Polyurethanes are thermally weak; an MDI-based PU begins to lose volatiles at 190–200 °C [123]. Photoablation of polyurethanes (with 193, 248, and 308 nm laser light) has been demonstrated [124]. Estevam-Alves et al. used DLIP to produce surface structures on a PU based on MDI [117]. The diol is bio-based and biodegradable (castor oil [125]). DLIP produces periodic line surface structures with spatial periods ranging from 0.5 to 5.0 μm . Defect-free periodic line-like patterns (structure depths between 270 and 1250 nm) are produced. Two typical shapes (sinusoidal and sigmoidal-like) of trenches have been observed for the PU material, suggesting that the ablation process results from a combination of photothermal and photochemical processes. While the nonpatterned PU exhibited a water contact angle of 81°, it increased with the size of the period being of 102° for the 3 μm structure, in agreement with the model of Cassie-Baxter [89]. While most PU copolymers are based on aromatic diisocyanates (MDI or TDI), there are PU copolymers made with aliphatic diols and diisocyanates [126], where the only chromophore in the polymer will be the urethane group with low absorption even at 266 nm.



Scheme 3. Chemical structure of the comonomer units of copolymers used with DLIP.

2.2.2. Poly(styrene-co-acrylonitrile) (SAN)

SAN is a copolymer widely used in place of polystyrene owing to its greater thermal resistance. At low acrylonitrile contents, it is transparent in the visible region. However, at a high acrylonitrile content, charge-transfer complexes are formed between the nitrile group (from acrylonitrile) and the aromatic ring (from styrene), which absorb light in the near-UV range [127]. Moreover, the nitrile group could be chemically converted to amine ($-NH_2$), amide ($-CONH_2$), or carboxylic acid ($-COOH$), allowing for controlling the hydrophilicity, acid/base behavior, and/or conjugate biomolecules [128]. Polyacrylonitrile absorbs at 265 nm, owing to the presence of enamine resonant structures [129]. The polymer is thermally stable, degrading at ca. 300 °C [130]. PAN photoablation was studied [131], and it was found that light at 308 nm causes removal of the polymer, while light at 248 nm produces cyclization and light at 193 nm induces removal of the nitrile group. Broglia et al. [118] studied the structuring by DLIP (266 nm) of SAN copolymers with a different acrylonitrile content. The laser irradiation was produced by both direct ablation and collapse/swelling of the illuminated surface. By varying the laser fluence and the copolymer composition, the surface structure can be changed from a periodic pattern with a swelled topography to an ablated-like structure.

2.2.3. Poly(methylmethacrylate-co-styrene) (P(MMA-co-S))

The optical and thermal properties of styrene and MMA monomer units have been described above. The copolymerization changes significantly the patterns produced. When PMMA-PS is irradiated with relatively low laser fluences ($<300 \text{ mJ/cm}^2$), the regions at interference maxima positions (points by interference of three beams) expand upwards, obtaining a smooth protruding hemisphere. Either MMA monomer or volatile products [132] form bubbles that cannot be released from the material surface due to the persistence of the PS chains. At higher fluences, the bubbles burst open, creating craters in the surface.

2.2.4. Poly(styrene-co-glycidylmethacrylate) (P(S-co-GMA))

The copolymer contains styrene (PS) and acrylate (e.g., PMMA) units, whose properties have been described above. The epoxy unit (GMA) shows weak absorptions below

210 nm [133]; therefore, it likely does not contribute to the absorption spectra. Acevedo et al. used DLIP (266 nm) to pattern copolymers with a different ratio of S/GMA [64]. The surface of PS (homopolymer) is ablated at the position of maximum light intensity, while in the copolymers, the surfaces swell up at the regions with maximum illumination. This behavior is similar to that of P(S-co-MMA). The styrene units absorb the laser light, giving photothermally ablated regions or promoting the chemical decomposition of acrylate units. Therefore, DLIP provides a unique way to produce ordered structures protruding ridges (expansion) or trenches (ablation) while maintaining the copolymer chemical structure. Reacting the GMA groups with amine-terminated polyethyleneglycol-linked quantum dots allows for spatially localizing the fluorescent QD. In that way, a patterned and chemically reactive surface can be created using DLIP on P(S-co-GMA).

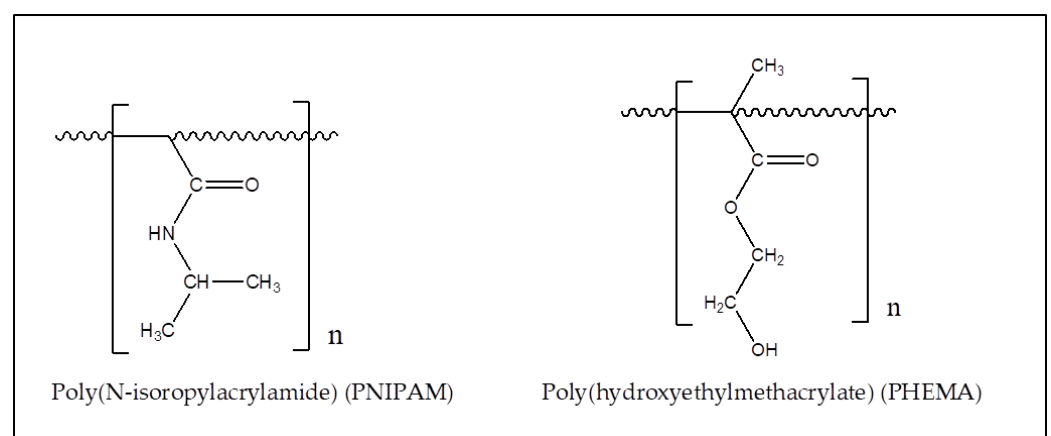
2.3. Hydrogels

Hydrogels are crosslinked polymers which retain large amount of water inside the 3D network. DLIP of those materials allow changing the optical or surface properties (Table 5).

Table 5. Summary of DLIP parameters used with synthetic hydrogels.

Polymer	Laser	λ (nm)	Fluence (mJ/cm ²)	Pulse Duration (ns)/Number	Setup	Refs.	Application
d-PNIPAM	Nd:YAG	355	800	10/1	MMI	[134]	Cell growth
Safrofilcon	–	263	470	4/4–7	DOE	[135]	Ophthalmic lenses
PANI@PNIPAM	Nd:YAG	266	400–800	10/1	MMI	[136]	Remote triggering
PHEMA PHEMA-UV	Nd:YAG	266		10/1	MMI	[137]	Ophthalmic diffraction gratings

The chemical structure of the main chains of the hydrogels used with DLIP is shown in Scheme 4. It should be mentioned that these hydrogels are cross-linked with bifunctional vinyl reactants. However, the fact that the cross-linker (e.g., BIS for PNIPAM) contains the same groups as the main chain polymer and that the amount present is low (<2%) allows for disregarding any effect of the cross-linker in DLIP. However, if a special cross-linker bearing chromophores (e.g., azo groups) is used, polymer ablation (and DLIP) of the hydrogel could be possible.



Scheme 4. Chemical structure of the monomer units of synthetic cross-linked hydrogels.

Hydrophilic synthetic gels (hydrogels) are important materials widely applied in biomedicine [138]. While there is a variety of polymer chemistry able to form hydrogels, the most common are polyacrylamides and polyacrylates. Polyacrylamides are intrinsically

hydrophilic (e.g., PNIPAM), while polyacrylate chain is hydrophobic and requires having a hydrophilic group (e.g., -OH in HEMA) in the monomer unit. As it was discussed above, polyacrylates can be photoablated (and structured by DLIP) using UV light (e.g., 266 nm), while polyacrylamide has no absorption above 240 nm [139] and is not ablated by 266 nm laser light.

2.3.1. PNIPAM

Therefore, a dye absorbing in the UV–VIS range is loaded inside PNIPAM (poly(*N*-isopropylacrylamide)) to allow DLIP structuring. Metal complexes with large organic ligands (e.g., $\text{Ru}(\text{bpy})_3^{+2}$ (Rubpy)) absorb strongly inside cross-linked acrylamides due to columbic and hydrophobic effects [140,141]. Molina et al. absorbed a Rubpy inside PNIPAM-cross-linked hydrogels and used DLIP to produce linear patterns by photothermal ablation in the dry gel [134]. The doping dye is used because PNIPAM has negligible absorption at 355 nm. The ridge pattern can be easily seen by optical and atomic force microscopy. However, upon swelling in aqueous solution, the ridge pattern disappears since the expansion closes the gaps. Moreover, since the material is a “smart” polymer, that is, it responds to external stimuli with volume changes, upon heating above the LCST of PNIPAM (32–33 °C [142]), the hydrogel partially collapses and the ridge pattern is restored. The changes are totally reversible, giving a way to change topography with external stimuli. Mulko et al. applied DLIP to structure a nanocomposite (PANI@PNIPAM) produced by in situ oxidative polymerization of aniline inside a PNIPAM cross-linked hydrogel [136]. The presence of PANI inside the transparent PNIPAM hydrogel network allowed for DLIP structuring at 355 nm. The DLIP resulted in a surface morphology of a nanofoam superimposed on a dominant line/groove pattern (dry state). Upon swelling in water, the trenches disappear since contiguous ridges moves together. However, since PANI is conductive, it can absorb radiofrequency (RF) radiation and heat up. When the temperature of PANI@PNIPAM increases above the LCST, the volume of the material collapses. The swelled flat surface of PANI@PNIPAM collapses, and the ridge/trench pattern recovers. The phenomenon is similar to that discussed above [136], but the change of roughness is remotely driven by RF, not by heating the whole system. PANI acts as both an absorber of light in DLIP and an absorber of RF in the triggering of thermosensitivity. Since any porous hydrogel could be modified by in situ polymerization of aniline (or other conductive polymer monomer-like pyrrole), the method could be used to allow direct patterning of other biocompatible gels (e.g., PDMS [74]).

2.3.2. Poly(hydroxyethylmethacrylate), PHEMA

PHEMA is one of the most widely used materials for soft contact lenses [143]. Sola et al. created linear periodic patterns on PHEMA by means of DLIP (266 nm) [139]. UV–VIS spectroscopy of PHEMA showed clear absorption in the UV region (cut-off at ca. 295 nm). Moreover, UV absorbers are usually added to the polymer to filter deleterious UV radiation to enter the eye. Such molecules shift the cut-off wavelength to ca. 400 nm. The analysis of the diffractive pattern (probed with a He-Ne laser at 632.8 nm) shows that the refractive index inside the patterned lines changes, compared with that of the bulk material, from 0.056 to 0.078 units, suggesting a densification of the remaining hydrogel. On the other hand, MicroRaman spectroscopy shows a very similar chemical structure in the patterned and virgin samples.

2.3.3. Safrofilcon A

A commercial ophthalmic hydrogel structured by DLIP, Safrofilcon is a proprietary material with unknown composition [137]. The regulatory declaration of the producer reveals that it contains several different acrylates and acrylamide monomer units without any additional group, which could absorb light in the UV range. However, the material could also contain molecules to filter UV in the eye, which have activity for DLIP. Sola et al. structured Safrofilcon A with DLIP to tune the refractive index of the ophthalmic

material [137]. A structured height and surface roughness increased with laser fluence, as shown by confocal microscopy. The structuring areas showed a delay in the hydration process, suggesting changes in the cross-linking structures. Micro-Raman spectroscopy show that at low laser fluences, the chemical structure of the polymer remained unaltered.

2.4. Conducting Polymers

Conducting polymers are interesting materials that show electronic conductivity, redox activity, and variable hydrophobicity [144]. Thin films can be deposited by in situ chemical (on any substrate) [145] or electrochemical (on conductive substrates) polymerization [146]. The fact that bands are broad likely allows even for photoablating with the 532 nm line (Table 6).

Table 6. Summary of the parameters used to structure conducting polymers using DLIP.

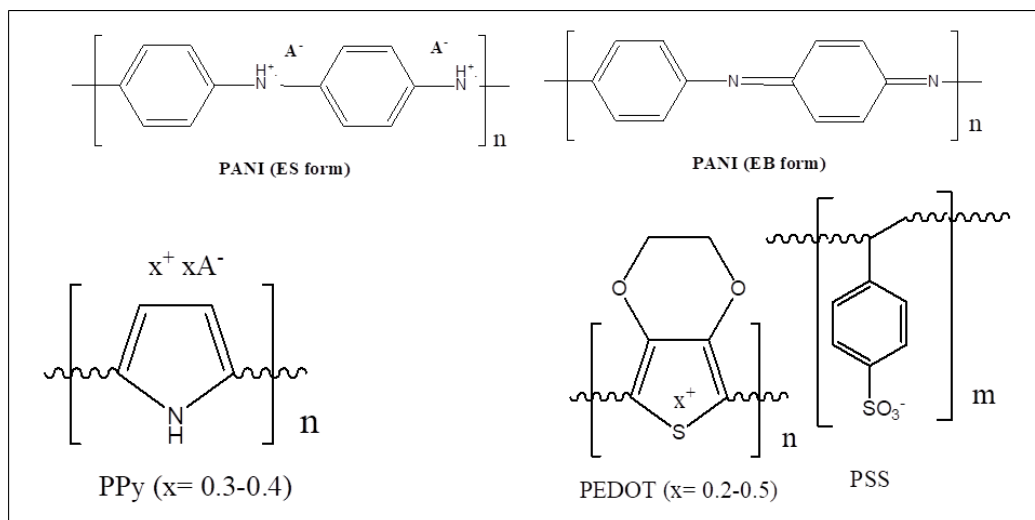
Polymer	Laser	λ (nm)	Fluence (mJ/cm ²)	Pulse Duration (ns)/Number	Setup	Refs.	Application
PANI	Nd:YAG	355	174–325	10/1	MMI	[147]	Conductive nanowires
PANI	Nd:YAG	355	174–325	10/1	MMI	[148]	Conductive arrays
PEDOT:PSS	Nd:YAG	355	54–296	10/1	MMI	[149]	Biomedicine
PPy	Nd:YAG	355	1200	10/1	MMI	[150]	Sensors

The conductivity of the polymer is not required for DLIP since deprotonated PANI (nonconductive) shows a similar UV–VIS spectrum (with some maxima shifts) and could act as a photothermal absorber [151]. This is relevant since there are plenty of “conductive” polymers that have low conductivity (e.g., poly(o-aminophenol), 5×10^{-3} S/cm [152]) but strong optical absorption [153], with bands at 340, 440 and 750 nm. Most conducting polymers have aromatic (homocyclic (e.g., PANI) or heterocyclic (e.g., PPy)) rings, which show ring $\pi \rightarrow \pi^*$ transitions (K and R bands of benzene) with large extinction coefficients in the UV (200–350 nm). Moreover, non-delocalized charged species (e.g., cation radicals) show absorption in the UV–VIS range (200–800 nm). The conductivity is associated with extended conjugation. The electronic transitions between the valence and conduction band of the organic metal absorb at even lower energies, in the red-NIR (600–1800 nm) region of the spectra. Therefore, conducting polymers (e.g., PANI) could absorb light at several lines used in DLIP (248, 266, 308, 355, and 1064 nm).

2.4.1. Polyaniline (PANI)

PANI is a conducting polymer produced by oxidative polymerization of aniline [154]. The monomer unit presents oxidized and reduced aromatic rings (Scheme 5), where the positive charge (radical cation) is compensated by mobile counterions (anions, A^-) in the emeraldine salt (ES) form. By deprotonation, the acid (A^-H^+) is lost, and a quinonimine uncharged form is present (emeraldine base (EB)). Both forms have aromatic rings and extended conjugation. Polyaniline absorbs light in the UV–VIS–NIR ranges [155]. PANI (ES form) shows a large absorption at 355 nm (α of ca. $73,000 \text{ cm}^{-1}$ at 350 nm [156]) and has low thermal stability with weight loss above 250 °C [157]. Lippert et al. studied the laser ablation of polyaniline (PANI) films at 308 nm (XeCl excimer laser) [158]. Upon successive pulses, the laser spots are ablated in the surface. Both PANI and modified polyanilines have transferred using LIFT [159], where PANI acts as both an absorbing layer and transferred material, which remains chemically unaltered and electroactive. PANI thin film have been structured using DLIP [147,148]. Thin films (ca. 200 nm) were deposited on flat PC and PI by oxidative polymerization of aniline in solution. The films were structured using laser (QS Nd:YAG, 10 ns) light (tripled frequency to 355 nm) in a two-beam DLIP setup. The PANI lines showed little degradation and remained conductive. The width of the ablated regions depends on the fluence of the laser light. At low fluences, only the light that surpasses an

intensity threshold is able to ablate the film. An EDS profile shows the presence of chlorine atoms (from the Cl^- counterions (X^-) of PANI (Scheme 5)) only in the nonablated region, suggesting complete removal of PANI above the light intensity threshold. In the case of PANI deposited onto PC, which does not absorb at 355 nm, only removal of the CP is observed. On the other hand, PI is also removed below PANI, creating subsurface trenches in the substrate and leaving the nonablated PANI on top of PI terraces. It seems that the energy absorbed by the thin film is not enough to melt or decompose the substrate (e.g., PC) and direct absorption is required (e.g., PI). Lasagni et al. uses a similar method to produce submicrometric conducting wire arrays of PANI [148]. Since the conductivity of PANI depends on different factors: redox state [160], pH [161], humidity [162], and concentration of organic vapors in the gas phase [162], the arrays can be used as miniature resistive chemical sensors. The electrical resistance of the array is found to be inversely proportional to the widths of the PANI strips, which are inversely proportional to the laser fluence [163]. Therefore, electrical resistors with predetermined resistance can be manufactured by short (10 ns) laser pulses, by just regulating the laser fluence. The method could be applied in laser trimming [164]. Besides its electrical properties, PANI is a hydrophilic and weakly acidic (pKa of ES form = 4–5) material with effects on cell growth/adhesion [165]. As it was discussed for conventional polymers, surface structuring has a large effect on surface wetting and growth/adhesion of cells. Gallarato et al. deposited chemically PANI films on PET [166]. They studied the formation of biofilms by a bacteria, *Pseudomonas aeruginosa*, on PANI surfaces before and after structuring using DLIP. The bacterial biofilm formation clearly decreased on PANI compared with the substrate (PET). Upon microstructuring the PANI thin films, even less biofilm formation was found [166]. The synergic effect of PANI coverage and structuring could be used to inhibit bacterial contamination in medical devices [165–167]. Nanofilms (<100 nm) of conducting polymers can be easily manufactured by electrochemical polymerization [168].



Scheme 5. Chemical structure of the conducting polymers structured with DLIP.

Thin films of PANI were electrochemically deposited on gold and structured by DLIP [148]. While PANI could be chemically deposited PANI thin films can be also deposited chemically on glass, a conductive (Au, Pt, GC, ITO) substrate is required to electropolymerize the monomer [168,169], but such electrical conductors absorb light and can also be structured by DLIP [170]. The structured film shows the same electrochemical response than plain PANI. Since electrochemistry is a quite sensitive technique to detect PANI degradation [146], these results confirm that DLIP does not degrade the nonilluminated regions of PANI. No underlayer effects (like those found on PANI/PI) were found, and PANI was completely ablated from the illuminated areas, leaving a clean metal substrate. It

seems that the lower thermal stability of PANI (degradation threshold at 250 °C) compared with Au (melting point at 1064 °C), combined with the higher thermal conductivity of the metal, allows for dissipating the energy, leaving the substrate undamaged. Since the metal substrate is unblocked in some regions, further electrochemistry in those areas is possible. The structures were used as a template to electrochemically deposit platinum nanoparticles in the gold bare areas [170]. Since PANI is not conductive in basic medium, the electrodeposition was carried out at pH = 11 to ensure that Pt nanoparticles deposited only on the uncovered areas and not on PANI. The mask made of PANI (EB form), which is soluble in NMP, was then removed, leaving strips of Pt NPs, as a negative image of the original DLIP pattern on PANI. Since Pt is electrocatalytic for methanol oxidation [171], while Au is not, the array of NP deposits act as an array of microelectrodes. Indeed, the structured electrode shows a current density for methanol oxidation ca. 5 times larger than a nonstructured one [170].

2.4.2. Polypyrrole (PPy)

PPy is a conducting polymer produced by oxidative polymerization of pyrrole [172]. Since it retains conductivity at neutral pH, it is widely used in biomedical applications [173]. PPy shows absorption bands at 310, 825, and 1375 nm (broad) [174]. The polymer degrades thermally above 180–200 °C [175]. While there is evidence of photothermal heating of PPy (800 nm) [176], in the best of our knowledge, no evidence of PPy photoablation seems to exist. Acevedo et al. used DLIP (355 nm) to structure large (>5 mm²) areas of polypyrrole (PPy) thin films deposited onto PP or PE [150]. Nanometric arrays of lines (>600 nm) or grids of PPy are produced. It is shown that only the PPy film is structured, while the substrate remains unaltered. FTIR and UV–VIS spectra remain unaltered after the structuration process. Contact angle measurement shows that the wettability is affected by the structuring, making the surface more hydrophobic.

2.4.3. Poly(3,4-ethylenedioxythiophene) Poly(styrenesulfonate) (PEDOT:PSS)

PEDOT is a conducting polymer produced by the oxidative polymerization of a modified thiophene [177]. Since one of the weaknesses of poly(thiophene) is the fast degradation by nucleophilic addition to the β positions in the ring [178], blocking those position as in PEDOT produces a more stable polymer. It is usually produced as a composite with poly(styrenesulfonate) (PSS). PEDOT:PSS has bands in the UV–VIS–NIR spectrum: one strong below 200 nm, which extends to longer wavelengths; a clear shoulder at 230 nm (UV); and a broad band with a maximum above 900 nm (NIR) [177]. PEDOT:PSS degrades thermally above 120 °C [179,180]. Indeed, photoablation of PEDOT:PSS (ps laser, 532 and 355 nm light) has been demonstrated [181]. Lasagni et al. used DLIP (355 nm, 10 ns) to structure electrochemically deposited PEDOT:PSS thin films [149]. The polymer blend (PEDOT:PSS) could be electrodeposited to small (<100 nm) to large thickness (>2 μ m). Therefore, the structuring of the PEDOT:PSS upper surface without leaving bare substrate regions could be tried. PEDOT has relatively low absorption at a light of 355 nm. In fact, the largest absorption of the conductive form is above 650 nm [182]. In the DLIP of PEDOT:PSS [149], the ablation efficiency of the laser was evaluated by applying single-laser pulses (without interference) and measuring the effect of laser fluence on the ablated spot radius [183]. Since the laser light has a Gaussian spatial profile of intensity, at lower fluences, only the central part of the beam has enough intensity to ablate the polymer. Therefore, the radius of the ablated spot is proportional to the ablation efficiency. In that way, the maximum fluence that ablates the PEDOT:PSS without ablating the metal film is measured and depends on the thickness of the PEDOT:PSS film. The threshold fluences are roughly double for the single-beam experiment compared with the double-beam (DLIP) setup since the maximum intensity of the interference pattern has double the intensity of the single beam.

3. Conclusions

The results reviewed show that DLIP is a simple and fast technique to create patterns on polymer surfaces. Different common polymers (PI, PC, PET) can be structured using UV laser light (266 and 355 nm). Other common polymers (PS, PMMA) can be structured by DLIP at 266 nm but not at 355 nm due to the negligible optical absorption. However, they (PS, PMMA, PMAA) can be structured at 355 nm by doping with azo dyes or with metal (Ag) clusters. The enhanced optical absorption at 355 nm allows structuring by DLIP. Copolymerization of nonabsorbing monomer units (e.g., alkyl chains) with monomers having chromophores (e.g., ciano groups) allows the structuring of the copolymers. Simple ablation involves the removal of a polymer from the surface, leaving depressed regions. On the other hand, some polymers release a monomer (e.g., PMMA) or produce gases (e.g., PAN). At high fluences, trenches (or holes) with fractured ridges are formed. At lower fluences, the gas releases under the surface expand the polymer, creating protruding smooth shapes. The softening of the polymer induced by the heat release related to light absorption helps to form the shapes. The same fluence-dependent shape forming will occur in the spot of single beams, suggesting that single-beam irradiation should be a first step to check the feasibility and shape the outcome of DLIP structuring of new polymer materials.

The structuring of conducting polymers (PANI, PPy, PEDOT:PSS) has been used to produce arrays of conducting nanowires with application as sensors. Since conducting polymers bear extended conjugated chains, with $\pi \rightarrow \pi^*$ transitions, and electron-band-related electronic transitions, they absorb in the UV (266 nm), near UV (355 nm), visible (532 nm), and NIR (1064 nm) lines (with frequency doubling) of Nd:YAG laser light. However, only DLIP structuring at 266 and 355 nm has been demonstrated. Depending on the optical properties of the polymer substrate where the CP is deposited, simple wires (or dots) are deposited on flat surfaces (nonabsorbing substrate) or nanowires (nanodisc) suspended on top of receding surfaces.

The structuring of the surfaces changes the wetting by water since Cassie-Baxter effects become operative. Since DLIP is likely the fastest (<5 s) surface structuring technique, large areas can be structured by 2D sequential drawing with laser pulses. Moreover, since lower fluences are required to structure polymers than metals or ceramics, the beams could be defocused and relatively large spots structured in each pulse. As it was discussed above, the maximum intensity of the pattern is the product of the laser fluence by the number of beams. Structuring thin films of special polymers (e.g., conducting polymers) deposited on transparent or absorbing substrates allow for not only creating structures with different topographic features (e.g., height) but differencing also in physicochemical properties (e.g., hydrophobicity). Changing the wettability of large areas could be applied in control of ice formation, lubrication, and microfluidic open channels.

Conducting polymers can be easily deposited (chemically or electrochemically) on metal substrates. Upon structuring, the film is removed of certain areas, and the exposed metal could act as a structured electrochemical electrode. The method was used with success to create structured deposits of active Pt nanoparticles on gold, which showed higher activity towards electrochemical methanol oxidation than nonstructured deposits. The combination of easy structuring and CPs special properties could be used to build switchable diffraction gratings by modulating the CP electrochromic properties.

Moreover, wettability has a strong effect on cell adhesion and biofilm growth, and DLIP has been used with success in controlling (or inhibiting) bacterial cell growth. Since biological cells are micrometric-sized objects, the submicrometric surface pattern gives rise to that liquid/surface interaction effects. On the other hand, structures (e.g., trenches of several micrometers width) could be fabricated using low (<20°) angles in the near UV, visible, or NIR. Such relatively large structures could be colonized by biological cells, which not only grow inside the structures, but the shape and direction of the trenches could induce the differentiation of planktonic cells into special tissue (e.g., fibroblasts).

DLIP structuring of synthetic hydrogels (PNIPAM, PHEMA) is not possible in the UV since the material is weakly absorbing. However, being highly swelled by water could be

easily doped by absorbing soluble dyes or loading with CPs by in situ polymerization. In that way, DLIP was used to structure the hydrogels. The structure made in the dry state is reversibly erased by isotropic swelling due to water absorption. In the case of “smart” (thermosensitive) hydrogels that collapse upon heating, the topography is nearly restored by gel collapse upon heating (LCST). DLIP structuring of nanocomposites (promoted by doping with dyes or conducting polymer/metal nanoparticles) allows producing smart surfaces whose topography can be controlled by heating or radiofrequency irradiation (remote). Moreover, commercial optical hydrogels can be efficiently structured by DLIP to produce optical elements with materials complying health regulations.

The patterned surfaces have also been used as optical (reflective/refractive) gratings. In that case, doping with dyes that absorb in the visible region is precluded, but there are molecules (e.g., polycyclic aromatics) that absorb in 355 nm but are transparent in the visible. Besides optical applications, gratings that generate large optical images by illumination could be used as unique signatures to avoid counterfeiting. Moreover, by structuring copolymers containing inert (e.g., styrene) and reactive (e.g., glycidylmethacrylate) monomer units, it is possible to manufacture polymer surfaces with topographic and chemical reactivity patterning. By reaction with fluorescent nanoparticles (quantum dots), it is possible to map the reactivity pattern.

The three important parameters in polymer science are mean molecular weight, crystallinity, and glass transition temperature (T_g). No attempt has been made to correlate those parameters with the feasibility of DLIP structuring. However, it seems that those parameters do not affect DLIP since the photoablation occurs in a short time at a temperature much higher than the T_g and both noncrystalline and crystalline regions sublime or degrade. However, it is reasonable that low-molecular-weight polymer chains (present in the chain length distribution of polydisperse polymer chains) sublime/degrade faster and swell the polymer. Further research in the subject is required.

Since most common polymers do not absorb light at 266 nm, the use of picosecond lasers could allow for two-photon absorption to occur. However, high fluences are required, and frequency-doubling crystals have low efficiency with ps laser. Therefore, fundamental (NIR, 1064 nm) laser lines were used. Two-photon absorption of 1064 nm light matches a transition wavelength (532 nm), where most common polymers do not absorb. However, a successful DLIP has been performed with 1064 nm with PS, PI, and PC(BPA). A possible explanation is that harmonics of vibrational (infrared) bands (e.g., C-H stretching) fall in the 1000–1100 nm region and can absorb NIR (1064 nm) light. If that is the case, other common polymers (e.g., PP) could be photoablated (and structured by DLIP) with 1064 nm picosecond light.

It can be seen that most DLIP work has been performed by experimentally trying the conditions. However, it would be advisable to use the previous experience with photoablation of polymers to design the DLIP experiments, in terms of light wavelength, fluence, and use of a dopant. Moreover, experimental trials using single-beam pulses at different fluences will give relevant information to plan the DLIP work.

4. Future Endeavors

While DLIP has been applied to different types of polymers with success, the technique has not been tried on widely used polymers. The evidence of successful polymer laser photoablation is a good guide to the possible application of DLIP to structure polymer surfaces. In Table 7 are shown common polymers where laser photoablation in the UV range has been demonstrated and DLIP could be used.

Table 7. Evidence of successful laser ablation of common polymers.

Polymer	Pulse Duration	λ (nm)	Doping	Ref.
PTFE		308 266	Perfluoro-s-triazines	[184]
PVC	4–6 ns	266	None	[185]
Polyamide (Nylon 6,6)	17 ns	308	None	[186]
	400 μ s	1060		
P(α -MeS)	15 ns	193	None	[187]
ABS	15 ns	248	None	[188]
	100 fs	800	None	
ABS/PVC	60 ps	266	None	[189]
Polyetherimide	60 ns	355	None	[190]
PP	130 fs	800	None	[191]
PE	64 ns	1064	Black pigment	[192]
Polythiophene	CW	325	None	[193]
PCL	35 ns	193	None	[194]
	220 fs	800		
PCL/gelatin nanofiber	150 fs	775	None	[195]
Nitrocellulose	5 ns	337	Stilbene 420, Coumarin 120, Rhodamine 6G	[33]
Polyurethane (PU) + Poly(lactic-co-glycolic acid) (PLGA) + Poly(lactide-polyethylene glycol-poly(lactide) (PPP)	200 fs	75	None	[196]

Moreover, conjugated polymers (POAP, PPD, PCBz, PTPA, PTh, PPV, PCBz, PTPA, PDA) could be ablated using UV (266 and 355 nm) light and visible (532 nm) and NIR (1064 nm). Other important but transparent polymers (CE, CHI, CMC, HPC, PVA, PEG, PEO, PDMS) could be structured by doping with UV-absorbing dyes (e.g., triazine dyes) or metal/conducting polymer nanoparticles. Transparent solid polyelectrolytes (c-PAA, c-PAMPS, c-PDAMAC) could be easily doped with charged dyes (e.g., methyl red (-) for PDAMAC (+)), which act as counterions of the fixed charges. Once the dyes have been used as light absorber, it can be removed by ion exchange with a nonabsorbing dye (e.g., Na⁺).

More complex polymeric systems—porous organic frameworks (POFs) [197] or dendronized polymers [198]—could be structured by DLIP since the building blocks contain chromophores enabling polymer ablation.

From the point of view of the thin films and surfaces, self-assembled monolayers (SAM) [199], layer-by-layer (LbL) multilayers [200], and Langmuir–Blodgett monolayers [201] should be easily structured by DLIP, creating 2 D and 3D structures with novel properties.

The work in DLIP of polymers have given place to patents of invention [202,203].

Author Contributions: C.A.B. and D.F.A. contributed equally to the manuscript. All authors have read and agreed to the published version of the manuscript.

Funding: This research received no external funding.

Acknowledgments: Both authors are permanent researchers of CONICET.

Conflicts of Interest: The authors declare no conflict of interest.

Abbreviations

ABS	poly(acrylonitrile-butadiene-styrene)
CE	cellulose
CHI	chitosan
CMC	carboxymethylcellulose
CP	conductive polymer
c-PAA	cross-linked poly(acrylic acid)
c-PAMPS	poly(2-acrylamido-2-methylpropanesulfonic acid)
c-PDAMAC	cross-linked polydiallyldimethylammonium chloride
DOE	diffractive optical element
EDS	energy dispersive X-ray spectroscopy
GC	glassy carbon
GMA	glycidylmethacrylate
HPC	hydroxypropylcellulose
ITO	indium tin oxide
LIFT	laser-induced forward transfer
LIPSS	laser-induced periodic surface structures
MMA	methylmethacrylate
MMI	modified Michelson interferometer
NCel	nitrocellulose
NIR	near-infrared range (800–2400 nm)
NMP	N-methylpyrrolidone
P(α -MeS)	poly(α -methylstyrene)
PA	poly(amide) (nylon 66)
PAN	polyacrylonitrile
PBT	polybutylene terephthalate
PC (BPA)	polycarbonate (with bisphenol A as diol)
PC	polycarbonate
PCBz	Polycarbazole
PDA	poly(dopamine)
PDMS	poly(dimethylsiloxane)
PE	polyethylene
PEDOT	poly(ethylenedioxythiophene)
PEEK	poly(ether ether ketone)
PEG	poly(ethyleneglycol)
PEN	poly(ethylene 2,6-naphthalate)
PEO	poly(ethyleneoxide)
PET	poly(ethyleneterephthalate)
PHEMA	poly(hydroxyethylmethacrylate)
PI	polyimide
PLA	polylactic acid
PMAA	poly(methacrylic acid)
PMMA	poly(methylmethacrylate)
PNIPAM	poly(N-isopropylacrylamide)
POAP	poly(o-aminophenol)
POM	polyoxymethylene
PP	polypropylene
PPD	poly(phenylenediamine)
PPV	poly(phenylenevinylene)
PPy	polypyrrole
PS	polystyrene
PSS	poly(styrene sulfonate)
PTh	polythiophene
PTPA	poly(triphenylamine)
PTT	poly(trimethyleneterephthalate)
PVA	poly(vinyl alcohol)
PVAc	poly(vinylacetate)

SAN	poly(styrene-co-acrylonitrile)
UV	ultraviolet range (200–380 nm)
Vis	visible range (380–800 nm)
α	coefficient of light intensity attenuation (cm^{-1})
ε	molar extinction coefficients ($\text{M}^{-1} \text{cm}^{-1}$)

References

- Voisiat, B.; Wang, W.; Holzhey, M.; Lasagni, A.F. Improving the homogeneity of diffraction based colours by fabricating periodic patterns with gradient spatial period using Direct Laser Interference Patterning. *Sci. Rep.* **2019**, *9*, 7801. [[CrossRef](#)]
- Berendsen, C.W.J.; Škerek, M.; Najdek, D.; Černý, F. Superhydrophobic surface structures in thermoplastic polymers by interference lithography and thermal imprinting. *Appl. Surf. Sci.* **2009**, *255*, 9305–9310. [[CrossRef](#)]
- Samal, S.; Tyc, O.; Heller, L.; Šittner, P.; Malik, M.; Poddar, P.; Catauro, M.; Blanco, I. Study of interfacial adhesion between nickel-titanium shape memory alloy and a polymer matrix by laser surface pattern. *Appl. Sci.* **2020**, *10*, 2172. [[CrossRef](#)]
- Lomba, M.; Oriol, L.; Sánchez-Somolinos, C.; Gražú, V.; Moros, M.; Serrano, J.L.; De La Fuente, J.M. Cell adhesion on surface patterns generated by the photocrosslinking of hyperbranched polyesters with a trisdiazonium salt. *React. Funct. Polym.* **2013**, *73*, 499–507. [[CrossRef](#)]
- Alikhani, A.; Fathollahzadeh, M.; Hajihosseini, H.; Fathipour, M. An interesting route using electron-beam lithography and photolithography to pattern submicron interdigitated electrodes array for sensing applications. *J. Iran. Chem. Soc.* **2020**, *17*, 187–194. [[CrossRef](#)]
- Deku, F.; Cohen, Y.; Joshi-Imre, A.; Kanneganti, A.; Gardner, T.J.; Cogan, S.F. Amorphous silicon carbide ultramicroelectrode arrays for neural stimulation and recording. *J. Neural Eng.* **2018**, *15*, 016007. [[CrossRef](#)]
- Proust, V.; Kirscher, Q.; Nguyen, T.K.N.; Obringer, L.; Ishii, K.; Rault, L.; Demange, V.; Berthebaud, D.; Ohashi, N.; Uchikoshi, T.; et al. Hafnium Oxide Nanostructured Thin Films: Electrophoretic Deposition Process and DUV Photolithography Patterning. *Nanomaterials* **2022**, *12*, 2334. [[CrossRef](#)]
- Lee, J.Y.; Kim, E.A.; Han, J.; Choi, Y.-H.; Hahm, D.; Kang, C.J.; Bae, W.K.; Lim, J.; Cho, S.-Y. Nondestructive Direct Photolithography for Patterning Quantum Dot Films by Atomic Layer Deposition of ZnO. *Adv. Mater. Interfaces* **2022**, *9*, 2200835. [[CrossRef](#)]
- Duay, J.; Goran, J.M.; Stevenson, K.J. Facile fabrication of carbon ultramicro- to nanoelectrode arrays with tunable voltammetric response. *Anal. Chem.* **2014**, *86*, 11528–11532. [[CrossRef](#)] [[PubMed](#)]
- Hong, H.; Kim, D.S. Robust topographical micro-patterning of nanofibrillar collagen gel by in situ photochemical crosslinking-assisted collagen embossing. *Nanomaterials* **2020**, *10*, 2574. [[CrossRef](#)]
- Fu, Y.; Soldera, M.; Wang, W.; Voisiat, B.; Lasagni, A.F. Picosecond laser interference patterning of periodical micro-architectures on metallic molds for hot embossing. *Materials* **2019**, *12*, 3409. [[CrossRef](#)] [[PubMed](#)]
- Sajfutdinow, M.; Uhlig, K.; Prager, A.; Schneider, C.; Abel, B.; Smith, D.M. Nanoscale patterning of self-assembled monolayer (SAM)-functionalised substrates with single molecule contact printing. *Nanoscale* **2017**, *9*, 15098–15106. [[CrossRef](#)] [[PubMed](#)]
- Lang, V.; Roch, T.; Lasagni, A.F. World record in high speed laser surface microstructuring of polymer and steel using direct laser interference patterning. *Proc. SPIE Int. Soc. Opt. Eng.* **2016**, *9736*, 97360Z. [[CrossRef](#)]
- Nebel, C.E. Laser interference structuring of α -Si:H. *Mat. Res. Soc. Sym. Proc.* **1996**, *420*, 117–128. [[CrossRef](#)]
- Müller, D.W.; Fox, T.; Grützmacher, P.G.; Suarez, S.; Mücklich, F. Applying Ultrashort Pulsed Direct Laser Interference Patterning for Functional Surfaces. *Sci. Reps.* **2020**, *10*, 3647. [[CrossRef](#)] [[PubMed](#)]
- Fabris, D.; Lasagni, A.F.; Fredel, M.C.; Henriques, B. Direct laser interference patterning of bioceramics: A short review. *Ceramics* **2019**, *2*, 578–586. [[CrossRef](#)]
- Ilcisin, K.J.; Fedosejevs, R. Direct production of gratings on plastic substrates using 248-nm krf laser radiation. *Appl. Opt.* **1987**, *26*, 396–400. [[CrossRef](#)] [[PubMed](#)]
- Labeyrie, A.; Flamand, J. Spectrographic performance of holographically made diffraction gratings. *Opt. Commun.* **1969**, *1*, 5–8. [[CrossRef](#)]
- Lasagni, A.F.; Yuan, D.; Das, S. Layer-by-layer interference lithography of three-dimensional microstructures in SU. *Adv. Eng. Mater.* **2009**, *11*, 408–411. [[CrossRef](#)]
- Jurkevičiute, A.; Armakavičius, N.; Virganavičius, D.; Šimatonis, L.; Tamulevičius, T.; Tamulevičius, S. Fabrication and characterization of one- and two-dimensional regular patterns produced employing multiple exposure holographic lithography. *J. Optoelectron. Adv. M* **2017**, *19*, 119–126.
- Rößler, F.; Lang, V.; Günther, D.; Lasagni, A.F. Fabricating Three-Dimensional Periodic Micro Patterns on Photo-Resists Using Laser Interference Lithography. *Adv. Eng. Mater.* **2017**, *19*, 1600855. [[CrossRef](#)]
- Lee, D.; Kim, B.-Y.; Park, C.H.; Jeong, G.; Park, S.-D.; Yoo, M.J.; Yang, H.; Lee, W.S. Photocurable Three-Dimensional Printing Resin to Enable Laser-Assisted Selective Electroless Metallization for Customized Electronics. *ACS Appl. Polym. Mater.* **2021**, *3*, 4735–4745. [[CrossRef](#)]
- Mulko, L.; Soldera, M.; Lasagni, A.F. Structuring and functionalization of non-metallic materials using direct laser interference patterning: A review. *Nanophotonics* **2022**, *11*, 203–240. [[CrossRef](#)]
- Rebollar, E.; Castillejo, M.; Ezquerro, T.A. Laser induced periodic surface structures on polymer films: From fundamentals to applications. *Eur. Polym. J.* **2015**, *73*, 162–174. [[CrossRef](#)]

25. Rodríguez-Rodríguez, A.; Rebollar, E.; Soccio, M.; Ezquerro, T.A.; Rueda, D.R.; Garcia-Ramos, J.V.; Castillejo, M.; Garcia-Gutierrez, M.-C. Laser-Induced Periodic Surface Structures on Conjugated Polymers: Poly(3-hexylthiophene). *Macromolecules* **2015**, *48*, 4024–4031. [CrossRef]
26. Mezera, M.; Alamri, S.; Hendriks, W.A.P.M.; Hertwig, A.; Elert, A.M.; Bonse, J.; Kunze, T.; Lasagni, A.F.; Römer, G.-W.R.B.E. Hierarchical micro-/nano-structures on polycarbonate via uv pulsed laser processing. *Nanomaterials* **2020**, *10*, 1184. [CrossRef]
27. Philipp, H.R.; Cole, H.S.; Liu, Y.S.; Sitnik, T.A. Optical absorption of some polymers in the region 240–170 nm. *Appl. Phys. Lett.* **1986**, *48*, 192–194. [CrossRef]
28. Chuang, T.J.; Hiraoka, H.; Mödl, A. Laser-photoetching characteristics of polymers with dopants. *Appl. Phys. A Sol. Surf.* **1988**, *45*, 277–288. [CrossRef]
29. Aleksandrov, A.P.; Bityurin, N.M.; Genkin, V.N.; Rukhman, I.V. Polymethylmethacrylate photoetching kinetics and modification at 200–300 nm. *Sov. Microelect.* **1989**, *18*, 16–19.
30. Ouchi, I.; Nakai, I.; Kamada, M. Anisotropic absorption spectra of polyester films in the ultraviolet and vacuum ultraviolet regions. *Nucl. Instrum. Methods Phys. Res. B* **2003**, *199*, 270–274. [CrossRef]
31. Costela, A.; Figuera, J.M.; Florido, F.; García-Moreno, I.; Collar, E.P.; Sastre, R. Ablation of poly(methyl methacrylate) and poly(2-hydroxyethyl methacrylate) by 308, 222 and 193 nm excimer-laser radiation. *Appl. Phys. A Mater. Sci. Process* **1995**, *60*, 261–270. [CrossRef]
32. Lippert, T.; Yabe, A.; Wokaun, A. Laser ablation of doped polymer systems. *Adv. Mater.* **1997**, *9*, 105–119. [CrossRef]
33. Kosmidis, C.E.; Skordoulis, C.D. Dopant-enhanced ablation of nitrocellulose by a nitrogen laser. *Appl. Phys. A Sol. Surf.* **1993**, *56*, 64–68. [CrossRef]
34. Acevedo, D.F.; Miras, M.C.; Barbero, C.A. Combinatorial synthesis and screening of photochromic dyes and modified conducting polymers. In *Combinatorial and High-Throughput Discovery and Optimization of Catalysts and Materials*; Potyrailo, R.A., Maier, W.F., Eds.; CRC Press: Boca Raton, FL, USA, 2007; pp. 239–256. [CrossRef]
35. Nguyen, T.L.; Saleh, M.A. Thermal degradation of azobenzene dyes. *Results Chem.* **2020**, *2*, 100085. [CrossRef]
36. Fujiwara, H.; Fukumura, H.; Masuhara, H. Laser ablation of a pyrene-doped poly(methyl methacrylate) film: Dynamics of pyrene transient species by spectroscopic measurements. *J. Phys. Chem.* **1995**, *99*, 11844–11853. [CrossRef]
37. Stoll, L.; Rech, R.; Flôres, S.H.; Nachtigall, S.M.B.; de Oliveira Rios, A. Carotenoids extracts as natural colorants in poly(lactic acid) films. *J. Appl. Polym. Sci.* **2018**, *135*, 46585. [CrossRef]
38. Smith, C.P., Jr. Review of methods for coloring nonwovens. *Text. Chem. Color.* **1990**, *22*, 25–29.
39. Xu, J.; Zhang, G.; Wu, C.; Liu, W.; Zhang, T.; Huang, Y.; Rong, Y. Organic solvent assisted laser processing of transparent polymer films based on the swelling and penetration behavior. *Opt. Laser Technol.* **2022**, *150*, 107937. [CrossRef]
40. D’Couto, G.C.; Babu, S.V.; Egitto, F.D.; Davis, C.R. Excimer laser ablation of polyimide-doped poly(tetrafluoroethylene) at 248 and 308 nm. *J. Appl. Phys.* **1993**, *74*, 5972–5980. [CrossRef]
41. Jiang, L.J.; Maruo, S.; Osellame, R.; Xiong, W.; Campbell, J.H.; Lu, Y.F. Femtosecond laser direct writing in transparent materials based on nonlinear absorption. *MRS Bull.* **2016**, *41*, 975–983. [CrossRef]
42. Raudino, A.; Fragalà, M.E.; Compagnini, G.; Puglisi, O. Modeling of low-temperature depolymerization of poly (methyl methacrylate) promoted by ion beam. *J. Chem. Phys.* **1999**, *111*, 1721–1731. [CrossRef]
43. Stump, B.L.; Snyder, W.J. Thermal Degradation of Polyimides by Thermogravimetric Analysis. *High Perform. Polym.* **1989**, *1*, 247–262. [CrossRef]
44. Lasagni, A.; Cornejo, M.; Lasagni, F.; Muecklich, F. Laser ablation modeling of periodic pattern formation on polymer substrates. *Adv. Eng. Mater.* **2008**, *10*, 488–493. [CrossRef]
45. Baumann, R.; Alamri, S.; Aguilar-Morales, A.L.; Lasagni, A.F.; Kunze, T. Advanced remote laser cutting of battery foils using an interference approach. *Mater. Lett. X* **2022**, *14*, 100138. [CrossRef]
46. Lippert, T.H.; Wokaun, A.; Stebani, J.; Nuyken, O.; Ihlemann, J. Triazene polymers designed for excimer laser ablation. *Angew. Makromolek. Chem.* **1993**, *206*, 97–110. [CrossRef]
47. Chen, Y.; Zhou, Y.; Wang, Z. Improvement of the frequency-doubling efficiency of high-average-power lasers using multicrystal scheme with opposite thermal properties. *Results Phys.* **2017**, *7*, 3530–3536. Available online: <https://velocimetry.net/laser%20catalogues/quantel/Brilliant%20B%20Qswitched%20NdYAG%20oscillator.pdf> (accessed on 13 October 2022). [CrossRef]
48. Kuhnke, M.; Cramer, L.; Dyer, P.E.; Dickinson, J.T.; Lippert, T.; Niino, H.; Pervolaraki, M.; Walton, C.D.; Wokaun, A. F₂ excimer laser (157 nm) ablation of polymers: Relation of neutral and ionic fragment detection and absorption. *J. Phys. Conf. Ser.* **2007**, *59*, 625–631. [CrossRef]
49. Ishi-Hayase, J.; Ishihara, T. Fundamental optical properties of photonic crystal slabs in the strong coupling regime. *Semicon. Sci. Technol.* **2003**, *18*, S411–S418. [CrossRef]
50. Burnett, J.H.; Gupta, R.; Griesmann, U. Absolute refractive indices and thermal coefficients of CaF₂, SrF₂, BaF₂, and LiF near 157 nm. *Appl. Opt.* **2002**, *41*, 2508–2513. [CrossRef]
51. Phillips, H.M.; Callahan, D.L.; Sauerbrey, R.; Szabó, G.; Bor, Z. Sub-100 nm lines produced by direct laser ablation in polyimide. *Appl. Phys. Lett.* **1991**, *58*, 2761–2763. [CrossRef]
52. Phillips, H.M.; Callahan, D.L.; Sauerbrey, R.; Szabó, G.; Bor, Z. Direct laser ablation of sub-100 nm line structures into polyimide. *Appl. Phys. A Sol. Surf.* **1992**, *54*, 158–165. [CrossRef]

53. Dyer, P.E.; Farley, R.J.; Giedl, R.; Karnakis, D.M. Excimer laser ablation of polymers and glasses for grating fabrication. *Appl. Surf. Sci.* **1996**, *96–98*, 537–549. [[CrossRef](#)]
54. Lippert, T.; Gerber, T.; Wokaun, A.; Funk, D.J.; Fukumura, H.; Goto, M. Single pulse nm-size grating formation in polymers using laser ablation with an irradiation wavelength of 355 nm. *Appl. Phys. Lett.* **1999**, *75*, 1018–1020. [[CrossRef](#)]
55. Klein-Wiele, J.-H.; Simon, P. Fabrication of periodic nanostructures by phase-controlled multiple-beam interference. *Appl. Phys. Lett.* **2003**, *83*, 4707–4709. [[CrossRef](#)]
56. Li, P.; Bakowsky, U.; Yu, F.; Loebach, C.; Muecklich, F.; Lehr, C.-M. Laser ablation patterning by interference induces directional cell growth. *IEEE Trans. Nanobio.* **2003**, *2*, 138–145. [[CrossRef](#)]
57. Yu, F.; Li, P.; Shen, H.; Mathur, S.; Lehr, C.-M.; Bakowsky, U.; Muecklich, F. Laser interference lithography as a new and efficient technique for micropatterning of biopolymer surface. *Biomaterials* **2005**, *26*, 2307–2312. [[CrossRef](#)]
58. Müller-Meskamp, L.; Kim, Y.H.; Roch, T.; Hofmann, S.; Scholz, R.; Eckardt, S.; Leo, K.; Lasagni, A.F. Efficiency enhancement of organic solar cells by fabricating periodic surface textures using direct laser interference patterning. *Adv. Mater.* **2012**, *24*, 906–910. [[CrossRef](#)]
59. Perez-Hernandez, H.; Lasagni, A.F. Fast and efficient manufacturing method of one- and two-dimensional polyethylene terephthalate transmission diffraction gratings by direct laser interference patterning. *Polym. Eng. Sci.* **2012**, *52*, 1903–1908. [[CrossRef](#)]
60. Soldera, M.; Alamri, S.; Storm, S.; Kunze, T.; Lasagni, A.F. Maximizing the efficiency of laser-fabricated diffraction gratings on PET using direct laser interference patterning. *Proc. SPIE* **2020**, *11268*, 112680Z. [[CrossRef](#)]
61. Guenther, D.; Valle, J.; Burgui, S.; Gil, C.; Solano, C.; Toledo-Arana, A.; Helbig, R.; Werner, C.; Lasa, I.; Lasagni, A.F. Direct laser interference patterning for decreased bacterial attachment. *Proc. SPIE* **2016**, *9736*, 973611. [[CrossRef](#)]
62. Alamri, S.; Fraggelakis, F.; Kunze, T.; Krupop, B.; Mincuzzi, G.; Kling, R.; Lasagni, A.F. On the interplay of DLIP and LIPSS upon ultra-short laser pulse irradiation. *Materials* **2019**, *12*, 1018. [[CrossRef](#)] [[PubMed](#)]
63. Cuello, E.A.; Mulko, L.E.; Barbero, C.A.; Acevedo, D.F.; Yslas, E.I. Development of micropatterning polyimide films for enhanced antifouling and antibacterial properties. *Colloids Surf. B* **2020**, *188*, 110801. [[CrossRef](#)]
64. Acevedo, D.F.; Martínez, G.; Arana, J.T.; Yslas, E.I.; Muecklich, F.; Barbero, C.; Salavagione, H.J. Easy way to fabricate nanostructures on a reactive polymer surface. *J. Phys. Chem. B* **2009**, *113*, 14661–14666. [[CrossRef](#)]
65. Valle, J.; Burgui, S.; Langheinrich, D.; Gil, C.; Solano, C.; Toledo-Arana, A.; Helbig, R.; Lasagni, A.; Lasa, I. Evaluation of Surface Microtopography Engineered by Direct Laser Interference for Bacterial Anti-Biofouling. *Macromol. Biosci.* **2015**, *15*, 1060–1069. [[CrossRef](#)] [[PubMed](#)]
66. Ränke, F.; Baumann, R.; Voisiat, B.; Fabián Lasagni, A. High throughput laser surface micro-structuring of polystyrene by combining direct laser interference patterning with polygon scanner technology. *Mater. Lett. X* **2022**, *14*, 100144. [[CrossRef](#)]
67. Martín-Fabiani, I.; Riedel, S.; Rueda, D.R.; Siegel, J.; Boneberg, J.; Ezquerra, T.A.; Nogales, A. Micro- and submicrostructuring thin polymer films with two and three-beam single pulse laser interference lithography. *Langmuir* **2014**, *30*, 8973–8979. [[CrossRef](#)] [[PubMed](#)]
68. Acevedo, D.; Salavagione, H.; Lasagni, A.; Morallón, E.; Muecklich, F.; Barbero, C. SERS active surface in two steps, patterning and metallization. *Adv. Eng. Mater.* **2013**, *15*, 325–329. [[CrossRef](#)]
69. Alamri, S.; Lasagni, A.F. Direct laser interference patterning of transparent and colored polymer substrates: Ablation, swelling, and the development of a simulation model. *Proc. SPIE* **2017**, *10092*, 1009219. [[CrossRef](#)]
70. Alamri, S.; Lasagni, A.F. Development of a general model for direct laser interference patterning of polymers. *Opt. Express* **2017**, *25*, 9603–9616. [[CrossRef](#)] [[PubMed](#)]
71. Günther, K.; Sonntag, F.; Moritzer, E.; Hirsch, A.; Klotzbach, U.; Lasagni, A.F. Universal micromachining platform and basic technologies for the manufacture and marking of microphysiological systems. *Micromachines* **2017**, *8*, 246. [[CrossRef](#)] [[PubMed](#)]
72. Acevedo, D.; Lasagni, A.; Barbero, C.; Muecklich, F. Micro/nano fabrication of surface architectures on polymers and copolymers using direct laser interference patterning. *Mater. Res. Symp. Proc.* **2008**, *1054*, 7–12. [[CrossRef](#)]
73. Broglia, M.F.; Suarez, S.; Soldera, F.; Muecklich, F.; Barbero, C.A.; Bellingeri, R.; Alustiza, F.; Acevedo, D. Direct laser interference patterning of polystyrene films doped with azo dyes, using 355 nm laser light. *Appl. Surf. Sci.* **2014**, *300*, 86–90. [[CrossRef](#)]
74. Bremus-Koebberling, E.A.; Beckemper, S.; Koch, B.; Gillner, A. Nano structures via laser interference patterning for guided cell growth of neuronal cells. *J. Laser App.* **2012**, *24*, 042013. [[CrossRef](#)]
75. Mulko, L.E.; Rossa, M.; Aranguren-Abrate, J.P.; Pino, G.A. Micropatterning of fluorescent silver nanoclusters in polymer films by Laser Interference. *Appl. Surf. Sci.* **2019**, *485*, 141–146. [[CrossRef](#)]
76. Hauschwitz, P.; Jagdheesh, R.; Alamri, S.; Rostohar, D.; Kunze, T.; Brajer, J.; Kopeček, J.; Mocek, T. Fabrication of functional superhydrophobic surfaces on carbon fibre reinforced plastics by IR and UV direct laser interference patterning. *Appl. Surf. Sci.* **2020**, *508*, 144817. [[CrossRef](#)]
77. Nuyken, O.; Stebani, J.; Lippert, T.; Wokaun, A.; Stasko, A. Photolysis, thermolysis, and protolytic decomposition of a triazine polymer in solution. *Macromol. Chem. Phys.* **1995**, *196*, 751–761. [[CrossRef](#)]
78. Qiu, Y.; Zhang, S.; Li, Y. High ultraviolet sensitivity of phthalic acid esters with environmental friendliness after modification through pharmacophore modeling associated with the solvation effect. *Pol. J. Environ. Stud.* **2020**, *29*, 2303–2316. [[CrossRef](#)]
79. Dzieciół, M.; Trzeszczyński, J. Volatile products of poly(ethylene terephthalate) thermal degradation in nitrogen atmosphere. *J. Appl. Polym. Sci.* **2000**, *77*, 1894–1901. [[CrossRef](#)]

80. Novis, Y.; Pireaux, J.J.; Brezini, A.; Petit, E.; Caudano, R.; Lutgen, P.; Feyder, G.; Lazare, S. Structural origin of surface morphological modifications developed on poly(ethylene terephthalate) by excimer laser photoablation. *J. Appl. Phys.* **1988**, *64*, 365–370. [[CrossRef](#)]
81. Sangkhawasi, M.; Remsungnen, T.; Vangnai, A.S.; Maitarad, P.; Rungrotmongkol, T. Prediction of the Glass Transition Temperature in Polyethylene Terephthalate/Polyethylene Vanillate (PET/PEV) Blends: A Molecular Dynamics Study. *Polymers* **2022**, *14*, 2858. [[CrossRef](#)] [[PubMed](#)]
82. Morales-Huerta, J.C.; De Ilarduya, A.M.; Muñoz-Guerra, S. Poly(alkylene 2,5-furandicarboxylate)s (PEF and PBF) by ring opening polymerization. *Polymer* **2016**, *87*, 148–158. [[CrossRef](#)]
83. Ishida, H.; Wellinghoff, S.T.; Baer, E.; Koenig, J.L. Spectroscopic Studies of Poly[N,N'-bis(phenoxyphenyl)pyromellitimide]. Structures of the Polyimide and Three Model Compounds. *Macromolecules* **1980**, *13*, 826–834. [[CrossRef](#)]
84. Akinyi, C.; Longun, J.; Chen, S.; Iroh, J.O. Decomposition and flammability of polyimide graphene composites. *Minerals* **2021**, *11*, 168. [[CrossRef](#)]
85. Ortelli, E.E.; Geiger, F.; Lippert, T.; Wei, J.; Wokaun, A. UV-laser-induced decomposition of Kapton studied by infrared spectroscopy. *Macromolecules* **2000**, *33*, 5090–5097. [[CrossRef](#)]
86. Braun, R.; Nowak, R.; Hess, P.; Oetzmann, H.; Schmidt, C. Photoablation of polyimide with IR and UV laser radiation. *Appl. Surf. Sci.* **1989**, *43*, 352–357. [[CrossRef](#)]
87. Workman, J.J., Jr.; Weyer, L. *Practical Guide to Interpretive Near-Infrared Spectroscopy*; CRC: Boca Raton, FL, USA, 2008; p. 218.
88. Johnson, S.L.; Schriver, K.E.; Haglund, R.F.; Bub, D.M. Effects of the absorption coefficient on resonant infrared laser ablation of poly(ethylene glycol). *J. Appl. Phys.* **2009**, *105*, 024901. [[CrossRef](#)]
89. Cassie, A.B.D.; Baxter, S. Wettability of porous surfaces. *Trans. Faraday Soc.* **1944**, *40*, 546–551. [[CrossRef](#)]
90. Li, T.; Zhou, C.; Jiang, M. UV absorption spectra of polystyrene. *Polym. Bull.* **1991**, *25*, 211–216. [[CrossRef](#)]
91. Chaudhary, A.K.; Vijayakumar, R.P. Studies on biological degradation of polystyrene by pure fungal cultures. *Environ. Dev. Sustain.* **2020**, *22*, 4495–4508. [[CrossRef](#)]
92. Lemoine, P.; Blau, W.; Drury, A.; Keely, C. Molecular weight effects on the 248-nm photoablation of polystyrene spun films. *Polymer* **1993**, *34*, 5020–5028. [[CrossRef](#)]
93. Su, Z.; Bedolla-Valdez, Z.I.; Wang, L.; Rho, Y.; Chen, S.; Gonel, G.; Taurone, E.N.; Moulé, A.J.; Grigoropoulos, C.P. High-Speed Photothermal Patterning of Doped Polymer Films. *ACS Appl. Mater. Interfaces* **2019**, *11*, 41717–41725. [[CrossRef](#)] [[PubMed](#)]
94. Bityurin, N. Studies on laser ablation of polymers. *Annu. Rep. Prog. Chem. Sect. C Phys. Chem.* **2005**, *101*, 216–247. [[CrossRef](#)]
95. Beinhorn, F.; Ihlemann, J.; Luther, K.; Troe, J. Micro-lens arrays generated by UV laser irradiation of doped PMMA. *Appl. Phys. A Mater. Sci. Process* **1999**, *68*, 709–713. [[CrossRef](#)]
96. Mullen, P.A.; Searle, N.Z. The ultraviolet activation spectrum of polycarbonate. *J. Appl. Polym. Sci.* **1970**, *14*, 765–776. [[CrossRef](#)]
97. Artham, T.; Doble, M. Biodegradation of aliphatic and aromatic polycarbonates. *Macromol. Biosci.* **2008**, *8*, 14–24. [[CrossRef](#)] [[PubMed](#)]
98. Jang, B.N.; Wilkie, C.A.A. TGA/FTIR and mass spectral study on the thermal degradation of bisphenol A polycarbonate. *Polym. Degrad. Stab.* **2004**, *86*, 419–430. [[CrossRef](#)]
99. Kunz, T.H.; Stebani, J.; Ihlemann, J.; Wokaun, A. Photoablation and microstructuring of polyester carbonates and their blends with a XeCl excimer laser. *Appl. Phys. A Mater. Sci. Process.* **1998**, *67*, 347–352. [[CrossRef](#)]
100. Cardona, M.; Güntherodt, G. Light Scattering in Solids IV: Electronics Scattering, Spin Effects, SERS, and Morphic Effects. In *Topics in Applied Physics*; Springer: Berlin, Germany, 1984.
101. Madzharova, F.; Heiner, Z.; Kneipp, J. Surface-Enhanced Hyper Raman Spectra of Aromatic Thiols on Gold and Silver Nanoparticles. *J. Phys. Chem. C* **2020**, *124*, 6233. [[CrossRef](#)] [[PubMed](#)]
102. Rubin, B.S. Bisphenol A: An endocrine disruptor with widespread exposure and multiple effects. *J. Steroid Biochem. Mol. Biol.* **2011**, *127*, 27–34. [[CrossRef](#)]
103. Xu, J.; Feng, E.; Song, J. Renaissance of aliphatic polycarbonates: New techniques and biomedical applications. *J. Appl. Polym. Sci.* **2014**, *131*, 39822. [[CrossRef](#)]
104. El-Newehy, M.H.; Kim, H.Y.; Khattab, T.A.; El-Naggar, M.E. Production of photoluminescent transparent poly(methyl methacrylate) for smart windows. *Luminescence* **2022**, *37*, 97–107. [[CrossRef](#)]
105. Lee, S.Y.; Lim, H.S.; Lee, N.E.; Cho, S.O. Biocompatible UV-absorbing polymer nanoparticles prepared by electron irradiation for application in sunscreen. *RSC Adv.* **2019**, *10*, 356–361. [[CrossRef](#)] [[PubMed](#)]
106. Kang, B.-S.; Kim, S.G.; Kim, J.-S. Thermal degradation of poly(methyl methacrylate) polymers: Kinetics and recovery of monomers using a fluidized bed reactor. *J. Anal. Appl. Pyrol.* **2008**, *81*, 7–13. [[CrossRef](#)]
107. Srinivasan, R.; Braren, B.; Dreyfus, R.W.; Hadel, L.; Seeger, D.E. Mechanism of the ultraviolet laser ablation of polymethyl methacrylate at 193 and 248 nm: Laser-induced fluorescence analysis, chemical analysis, and doping studies. *J. Opt. Soc. B* **1986**, *3*, 785–791. [[CrossRef](#)]
108. Lippert, T. Interaction of photons with polymers: From surface modification to ablation. *Plasma Process. Polym.* **2005**, *2*, 525–546. [[CrossRef](#)]
109. Moneris, M.; Broglia, M.F.; Yslas, E.I.; Barbero, C.A.; Rivarola, C.R. Highly effective antimicrobial nanocomposites based on hydrogel matrix and silver nanoparticles: Long-lasting bactericidal and bacteriostatic effects. *Soft Matter* **2019**, *15*, 8059–8066. [[CrossRef](#)]

110. Panayotov, I.V.; Orti, V.; Cuisinier, F.; Yachouh, J. Polyetheretherketone (PEEK) for medical applications. *J. Mater. Sci. Mater. Med.* **2016**, *27*, 118. [[CrossRef](#)] [[PubMed](#)]
111. Li, H.M.; Fouracre, R.A.; Given, M.J.; Banford, H.M.; Wysocki, S.; Karolczak, S. The effects on polyetheretherketone and polyethersulfone of electron and γ irradiation. *IEEE Trans. Dielectr. Electr. Insul.* **1999**, *6*, 295–303. [[CrossRef](#)]
112. Patel, P.; Hull, T.R.; McCabe, R.W.; Flath, D.; Grasmeyer, J.; Percy, M. Mechanism of thermal decomposition of poly(ether ether ketone) (PEEK) from a review of decomposition studies. *Polym. Degrad. Stab.* **2010**, *95*, 709–718. [[CrossRef](#)]
113. Babu, S.V.; D' Couto, G.C.; Egitto, F.D. Excimer laser induced ablation of polyetheretherketone, polyimide, and polytetrafluoroethylene. *J. Appl. Phys.* **1992**, *72*, 692–698. [[CrossRef](#)]
114. Lippert, T.H.; Wokaun, A.; Stebani, J.; Nuyken, O.; Ihlemann, J. Dopant-induced laser ablation of PMMA at 308 nm: Influence of the molecular weight of PMMA and of the photochemical activity of added chromophores. *Angew. Makromol. Chem.* **1993**, *213*, 127–155. [[CrossRef](#)]
115. Bhatnagar, M.S. *A Textbook of Polymer Chemistry*; Chand Publishing: New Dehli, India, 2004.
116. Da Silva, A.C.; Semeano, A.T.S.; Dourado, A.H.B.; Ulrich, H.; De Torresi, S.I.C. Novel Conducting and Biodegradable Copolymers with Noncytotoxic Properties toward Embryonic Stem Cells. *ACS Omega* **2018**, *3*, 5593–5604. [[CrossRef](#)]
117. Estevam-Alves, R.; Günther, D.; Dani, S.; Eckhardt, S.; Roch, T.; Mendonca, C.R.; Cestari, I.N.; Lasagni, A.F. UV Direct Laser Interference Patterning of polyurethane substrates as tool for tuning its surface wettability. *Appl. Surf. Sci.* **2016**, *374*, 222–228. [[CrossRef](#)]
118. Broglia, M.F.; Acevedo, D.F.; Langheinrich, D.; Perez-Hernandez, H.R.; Barbero, C.A.; Lasagni, A.F. Rapid fabrication of periodic patterns on poly(styrene-co-acrylonitrile) surfaces using direct laser interference patterning. *Int. J. Polym. Sci.* **2015**, *2015*, 721035. [[CrossRef](#)]
119. Ates, M.; Karadag, S.; Eker, A.A.; Eker, B. Polyurethane foam materials and their industrial applications. *Polym. Int.* **2022**, *71*, 1157–1163. [[CrossRef](#)]
120. Somarathna, H.M.C.C.; Raman, S.N.; Mohotti, D.; Mutalib, A.A.; Badri, K.H. The use of polyurethane for structural and infrastructural engineering applications: A state-of-the-art review. *Constr. Build. Mater.* **2018**, *190*, 995–1014. [[CrossRef](#)]
121. Sikdar, P.; Dip, T.M.; Dhar, A.K.; Bhattacharjee, M.; Hoque, M.S.; Ali, S.B. Polyurethane (PU) based multifunctional materials: Emerging paradigm for functional textiles, smart, and biomedical applications. *J. Appl. Polym. Sci.* **2022**, *139*, e52832. [[CrossRef](#)]
122. Senevirathna, S.R.; Amarasinghe, D.A.S.; Karunaratne, V.; Koneswaran, M.; Karunanayake, L. Effect of microstructural arrangement of MDI-based polyurethanes on their photoproperties. *J. Appl. Polym. Sci.* **2019**, *136*, 47431. [[CrossRef](#)]
123. Allan, D.; Daly, J.; Liggat, J.J. Thermal volatilisation analysis of TDI-based flexible polyurethane foam. *Polym. Degrad. Stab.* **2013**, *98*, 535–541. [[CrossRef](#)]
124. Zafiropoulos, V.; Petrakis, J.; Fotakis, C. Photoablation of polyurethane films using UV laser pulses. *Opt. Quantum Electron.* **1995**, *27*, 1359–1376. [[CrossRef](#)]
125. Cassales, A.; Ramos, L.A.; Frollini, E. Synthesis of bio-based polyurethanes from Kraft lignin and castor oil with simultaneous film formation. *Int. J. Biol. Macromol.* **2020**, *145*, 28–41. [[CrossRef](#)] [[PubMed](#)]
126. Gürses, C.; Karaaslan-Tunç, M.G.; Keleştemur, Ü.; Balcıoğlu, S.; Gülgen, S.; Köytepe, S.; Ateş, B. Aliphatic Polyurethane Films Based on Hexamethylene Diisocyanate and Saccharides for Biocompatible Transparent Coating on Optic Medical Devices. *Starch/Staerke* **2022**, *74*, 2100214. [[CrossRef](#)]
127. Priddy, D.B. Thermal discoloration chemistry of styrene-co-acrylonitrile. *Adv. Polym. Sci.* **1995**, *121*, 122–154. [[CrossRef](#)]
128. Shakeri, A.; Jarad, N.A.; Khan, S.; F Didar, T. Bio-functionalization of microfluidic platforms made of thermoplastic materials: A review. *Anal. Chim. Acta* **2022**, *1209*, 339283. [[CrossRef](#)]
129. Friedlander, H.N.; Peebles, L.H., Jr.; Brandrup, J.; Kirby, J.R. On the chromophore of polyacrylonitrile. VI. Mechanism of color formation in polyacrylonitrile. *Macromolecules* **1968**, *1*, 79–86. [[CrossRef](#)]
130. Xue, T.J.; McKinney, M.A.; Wilkie, C.A. The thermal degradation of polyacrylonitrile. *Polym. Degrad. Stab.* **1997**, *58*, 193–202. [[CrossRef](#)]
131. Nishio, S.; Chiba, T.; Matsuzaki, A.; Sato, H. Preparation of polymer films by laser ablation of polyacrylonitrile: Significant dependence on ablation wavelengths. *Appl. Surf. Sci.* **1996**, *106*, 132–136. [[CrossRef](#)]
132. Krajnovich, D.J. Incubation and photoablation of poly(methyl methacrylate) at 248 nm. New insight into the reaction mechanism using photofragment translational spectroscopy. *J. Phys. Chem. A* **1997**, *101*, 2033–2039. [[CrossRef](#)]
133. Rogers, M.T. The Electric Moments and Ultraviolet Absorption Spectra of Some Derivatives of Cyclopropane and of Ethylene Oxide. *J. Amer. Chem. Soc.* **1947**, *69*, 2544–2548. [[CrossRef](#)]
134. Molina, M.A.; Rivarola, C.R.; Broglia, M.F.; Acevedo, D.F.; Barbero, C.A. Smart surfaces: Reversible switching of a polymeric hydrogel topography. *Soft Matter* **2012**, *8*, 307–310. [[CrossRef](#)]
135. Sola, D.; Milles, S.; Lasagni, A.F. Direct laser interference patterning of diffraction gratings in safrofilcon-a hydrogel: Fabrication and hydration assessment. *Polymers* **2021**, *3*, 679. [[CrossRef](#)]
136. Mulko, L.E.; Cuello, E.A.; Barbero, C.A.; Pino, G.A.; Molina, M.; Rossa, M. Remote radiofrequency triggering of topography changes in a surface micropatterned PANI@PNIPAM nanocomposite. *Appl. Surf. Sci.* **2020**, *509*, 145370. [[CrossRef](#)]
137. Sola, D.; Alamri, S.; Lasagni, A.F. UV Direct Laser Interference Patterning of Diffraction Gratings in Poly-Hydroxyethyl-Methacrylate Ophthalmic Polymers. *J. Laser Micro Nanoeng.* **2020**, *15*, 186–190. [[CrossRef](#)]

138. Ho, T.-C.; Chang, C.-C.; Chan, H.-P.; Chung, T.-W.; Shu, C.-W.; Chuang, K.-P.; Duh, T.-H.; Yang, M.-H.; Tyan, Y.-C. Hydrogels: Properties and Applications in Biomedicine. *Molecules* **2022**, *27*, 2902. [[CrossRef](#)]
139. Al Momani, F.A.; Örmeci, B. Measurement of polyacrylamide polymers in water and wastewater using an in-line UV-vis spectrophotometer. *J. Environ. Chem. Eng.* **2014**, *2*, 765–772. [[CrossRef](#)]
140. Rivarola, C.R.; Biasutti, M.A.; Barbero, C.A. A visible light photoinitiator system to produce acrylamide based smart hydrogels: Ru(bpy)⁺² as photopolymerization initiator and molecular probe of hydrogel microenvironments. *Polymer* **2009**, *50*, 3145–3152. [[CrossRef](#)]
141. Molina, M.A.; Rivarola, C.R.; Barbero, C.A. Evidence of hydrophobic interactions controlling mobile ions release from smart hydrogels. *Mol. Cryst. Liq. Cryst.* **2010**, *521*, 265–271. [[CrossRef](#)]
142. Rivero, R.; Alustiza, F.; Capella, V.; Liaudat, C.; Rodriguez, N.; Bosch, P.; Barbero, C.; Rivarola, C. Physicochemical properties of ionic and non-ionic biocompatible hydrogels in water and cell culture conditions: Relation with type of morphologies of bovine fetal fibroblasts in contact with the surfaces. *Colloids Surf. B* **2017**, *158*, 488–497. [[CrossRef](#)] [[PubMed](#)]
143. Zare, M.; Bigham, A.; Zare, M.; Luo, H.; Rezvani Ghomi, E.; Ramakrishna, S. PHEMA: An overview for biomedical applications. *Int. J. Mol. Sci.* **2021**, *22*, 6376. [[CrossRef](#)]
144. Zare, E.N.; Makvandi, P.; Ashtari, B.; Rossi, F.; Motahari, A.; Perale, G. Progress in Conductive Polyaniline-Based Nanocomposites for Biomedical Applications: A Review. *J. Med. Chem.* **2020**, *63*, 1–22. [[CrossRef](#)] [[PubMed](#)]
145. Monge, N.E.; Miras, M.C.; Barbero, C.A. High-throughput screening method to detect amphiphilic counterions able to solubilize conducting polymers. *J. Comb. Chem.* **2010**, *12*, 814–817. [[CrossRef](#)] [[PubMed](#)]
146. Planes, G.A.; Rodríguez, J.L.; Miras, M.C.; García, G.; Pastor, E.; Barbero, C.A. Spectroscopic evidence for intermediate species formed during aniline polymerization and polyaniline degradation. *PCCP* **2010**, *12*, 10584–10593. [[CrossRef](#)] [[PubMed](#)]
147. Acevedo, D.A.; Lasagni, A.F.; Barbero, C.A.; Mücklich, F. Simple fabrication method of conductive polymeric arrays by using direct laser interference micro-/nanopatterning. *Adv. Mater.* **2007**, *19*, 1272–1275. [[CrossRef](#)]
148. Lasagni, A.; Acevedo, D.; Barbero, C.; Muecklich, F. Fabrication of conductive polymeric arrays using direct laser interference micro/nano patterning. *Mater. Res. Symp. Proc.* **2008**, *1030*, 61–66. [[CrossRef](#)]
149. Lasagni, A.F.; Hendricks, J.L.; Shaw, C.M.; Yuan, D.; Martin, D.C.; Das, S. Direct laser interference patterning of poly(3,4-ethylene dioxothiophene)-poly(styrene sulfonate) (PEDOT-PSS) thin films. *Appl. Surf. Sci.* **2009**, *255*, 9186–9192. [[CrossRef](#)]
150. Acevedo, D.F.; Frontera, E.; Broglia, M.F.; Mücklich, F.; Miras, M.C.; Barbero, C.A. One step lithography of polypyrrole. *Adv. Eng. Mater.* **2011**, *13*, 405–410. [[CrossRef](#)]
151. Abel, S.B.; Gallarato, L.A.; Dardanelli, M.S.; Barbero, C.A.; Rivarola, C.R.; Yslas, E.I. Photothermal lysis of *Pseudomonas aeruginosa* by polyaniline nanoparticles under near infrared irradiation. *Biomed. Phys. Eng. Express* **2018**, *4*, 045037. [[CrossRef](#)]
152. Barbero, C.; Tucceri, R.I.; Posadas, D.; Silber, J.J.; Sereno, L. Impedance characteristics of poly-o-aminophenol electrodes. *Electrochim. Acta* **1995**, *40*, 1037–1040. [[CrossRef](#)]
153. Tucceri, R.I.; Barbero, C.; Silber, J.J.; Sereno, L.; Posadas, D. Spectroelectrochemical study of poly-o-aminophenol. *Electrochim. Acta* **1997**, *42*, 919–927. [[CrossRef](#)]
154. Beygisangchin, M.; Rashid, S.A.; Shafie, S.; Sadrollhosseini, A.R.; Lim, H.N. Preparations, properties, and applications of polyaniline and polyaniline thin films—A review. *Polymers* **2021**, *13*, 2003. [[CrossRef](#)] [[PubMed](#)]
155. Agrawal, V.; Singla, E.; Agnihotri, P.K. Modulation of optical properties of electrochromic device. *J. Mater. Sci. Mater. Electron.* **2022**, *33*, 21935–21954. [[CrossRef](#)]
156. Barbero, C.; Kötz, R. Nanoscale Dimensional Changes and Optical Properties of Polyaniline Measured by in Situ Spectroscopic Ellipsometry. *J. Electrochem. Soc.* **1994**, *141*, 859–865. [[CrossRef](#)]
157. Kulkarni, V.G.; Campbell, L.D.; Mathew, W.R. Thermal stability of polyaniline. *Synth. Met.* **1989**, *30*, 321–325. [[CrossRef](#)]
158. Lippert, T.; Raimondi, F.; Wambach, J.; Wei, J.; Wokaun, A. Surface modification and structuring of electrical conducting and isolating polyaniline films. *Appl. Phys. A Mater. Sci. Process* **1999**, *69*, S291–S293. [[CrossRef](#)]
159. Cavallo, P.; Coneo Rodriguez, R.; Broglia, M.; Acevedo, D.F.; Barbero, C.A. Simple fabrication of active electrodes using direct laser transference. *Electrochim. Acta* **2014**, *116*, 194–202. [[CrossRef](#)]
160. Nogueira Pedroza Dias Mello, H.J.; Mulato, M. Impedimetric and Capacitive Transducer Platform for Chemical Sensors Based on Electrodeposited Polyaniline Thin Films. *J. Phys. Chem. C* **2022**, *126*, 12222–12229. [[CrossRef](#)]
161. Huang, W.S.; MacDiarmid, A.G. Optical properties of polyaniline. *Polymer* **1993**, *34*, 1833–1845. [[CrossRef](#)]
162. Cavallo, P.; Acevedo, D.F.; Fuertes, M.C.; Soler-Illia, G.J.A.A.; Barbero, C.A. Understanding the sensing mechanism of polyaniline resistive sensors. Effect of humidity on sensing of organic volatiles. *Sens. Actuators B Chem.* **2015**, *210*, 574–580. [[CrossRef](#)]
163. Lasagni, A.F.; Acevedo, D.F.; Barbero, C.A.; Mücklich, F. Advanced design of conductive polymeric arrays with controlled electrical resistance using direct laser interference patterning. *Appl. Phys. A* **2008**, *91*, 369–373. [[CrossRef](#)]
164. Joshi Anil, G.; Sarma, G.H. SEM studies on laser trimmed resistors. *IETE J. Res.* **1982**, *28*, 494–497. [[CrossRef](#)]
165. Yslas, E.I.; Cavallo, P.; Acevedo, D.F.; Barbero, C.A.; Rivarola, V.A. Cysteine modified polyaniline films improve biocompatibility for two cell lines. *Mater. Sci. Eng. C* **2015**, *51*, 51–56. [[CrossRef](#)]
166. Gallarato, L.A.; Mulko, L.E.; Dardanelli, M.S.; Barbero, C.A.; Acevedo, D.F.; Yslas, E.I. Synergistic effect of polyaniline coverage and surface microstructure on the inhibition of *Pseudomonas aeruginosa* biofilm formation. *Colloids Surf. B* **2017**, *150*, 1–7. [[CrossRef](#)] [[PubMed](#)]

167. Li, X.; Sun, L.; Zhang, P.; Wang, Y. Novel approaches to combat medical device-associated biofilms. *Coatings* **2021**, *11*, 294. [[CrossRef](#)]
168. Barbero, C.; Zerbino, J.; Sereno, L.; Posadas, D. Optical properties of electropolymerized orthoaminophenol. *Electrochim. Acta* **1987**, *32*, 693–697. [[CrossRef](#)]
169. AlQattan, B.; Butt, H.; Sabouri, A.; Yetisen, A.K.; Ahmed, R.; Mahmoodi, N. Holographic direct pulsed laser writing of two-dimensional nanostructures. *RSC Adv.* **2016**, *6*, 111269–111275. [[CrossRef](#)] [[PubMed](#)]
170. Acevedo, D.F.; Salavagione, H.J.; Lasagni, A.F.; Morallón, E.; Mücklich, F.; Barbero, C. Fabrication of highly ordered arrays of platinum nanoparticles using direct laser interference patterning. *ACS Appl. Mater. Interfaces* **2009**, *1*, 549–551. [[CrossRef](#)] [[PubMed](#)]
171. Planes, G.A.; Rodríguez, J.L.; Pastor, E.; Barbero, C. Evidence of a free Pt surface under electrodeposited polyaniline (PANI) films: CO adsorption and methanol oxidation at PANI/Pt without metal particles. *Langmuir* **2003**, *19*, 8137–8140. [[CrossRef](#)]
172. Vernitskaya, T.V. Polypyrrole: A conducting polymer; its synthesis, properties and applications. *Russ. Chem. Rev.* **1997**, *66*, 443–457. [[CrossRef](#)]
173. Liang, Y.; Goh, J.C.-H. Polypyrrole-Incorporated Conducting Constructs for Tissue Engineering Applications: A Review. *Bioelectricity* **2020**, *2*, 101–119. [[CrossRef](#)]
174. Yakushi, K.; Lauchlan, L.J.; Clarke, T.C.; Street, G.B. Optical study of polypyrrole perchlorate. *J. Chem. Phys.* **1983**, *79*, 4774–4778. [[CrossRef](#)]
175. Omastova, M.; Rychlý, J.; Trchová, M.; Kovářová, J. Properties and thermal decomposition of polypyrrole prepared in the presence of sodium bis(2-ethylhexyl) sulfosuccinate. *Des. Monomers Polym.* **2004**, *7*, 633–646. [[CrossRef](#)]
176. Abel, S.B.; Rivarola, C.R.; Barbero, C.A.; Molina, M. Electromagnetic radiation driving of volume changes in nanocomposites made of a thermosensitive hydrogel polymerized around conducting polymer nanoparticles. *RSC Adv.* **2020**, *10*, 9155–9164. [[CrossRef](#)] [[PubMed](#)]
177. Gueye, M.N.; Carella, A.; Faure-Vincent, J.; Demadrille, R.; Simonato, J.-P. Progress in understanding structure and transport properties of PEDOT-based materials: A critical review. *Prog. Mater. Sci.* **2020**, *108*, 100616. [[CrossRef](#)]
178. Harada, H.; Fuchigami, T.; Nonaka, T. Degradation and its prevention, and the deactivation and reactivation of electroactive polythiophene films during oxidation/reduction cycles. *J. Electroanal. Chem.* **1991**, *303*, 139–150. [[CrossRef](#)]
179. Yemata, T.A.; Zheng, Y.; Kyaw, A.K.K.; Wang, X.; Song, J.; Chin, W.S.; Xu, J. Improved Thermoelectric Properties and Environmental Stability of Conducting PEDOT:PSS Films Post-treated with Imidazolium Ionic Liquids. *Front. Chem.* **2020**, *7*, 870. [[CrossRef](#)] [[PubMed](#)]
180. Stepien, L.; Roch, A.; Tkachov, R.; Leupolt, B.; Han, L.; van Ngo, N.; Leyens, C. Thermal operating window for PEDOT:PSS films and its related thermoelectric properties. *Synth. Met.* **2017**, *225*, 49–54. [[CrossRef](#)]
181. Karnakis, D.; Kearsley, A.; Knowles, M. Ultrafast laser patterning of OLEDs on flexible substrate for solid-state lighting. *J. Laser Micro Nanoeng.* **2009**, *4*, 218–223. [[CrossRef](#)]
182. Gustafsson, J.C.; Liedberg, B.; Inganäs, O. In situ spectroscopic investigations of electrochromism and ion transport in a poly(3,4-ethylenedioxythiophene) electrode in a solid state electrochemical cell. *Solid State Ion.* **1994**, *69*, 145–152. [[CrossRef](#)]
183. McDonald, J.P.; Hendricks, J.L.; Mistry, V.R.; Martin, D.C.; Yalisove, S.M. Femtosecond pulsed laser patterning of poly(3,4-ethylene dioxythiophene)-poly(styrenesulfonate) thin films on gold/palladium substrates. *J. Appl. Phys.* **2007**, *102*, 013107. [[CrossRef](#)]
184. Hiraoka, H.; Lazare, S.; Chuang, T.J.; Rettner, C.T.; Hunziker, H.E. Laser photoetching of doped poly(tetrafluoroethylene); substituted-PTFE, and polyimide films. *Microelectron. Eng.* **1991**, *13*, 429–432. [[CrossRef](#)]
185. Hemmerlin, M.; Mermet, J.M.; Bertucci, M.; Zydowicz, P. Determination of additives in PVC material by UV laser ablation inductively coupled plasma atomic emission spectrometry. *Spectrochim. Acta-Part B At. Spectrosc.* **1997**, *52*, 421–430. [[CrossRef](#)]
186. Skordoulis, C.D.; Makropoulou, M.; Serafetinides, A.A. Ablation of nylon-6,6 with UV and IR lasers. *Appl. Surf. Sci.* **1995**, *86*, 239–244. [[CrossRef](#)]
187. Burrel, M.C.; Liu, Y.S.; Cole, H.S. An X-ray photoelectron spectroscopy study of poly(methylmethacrylate) and poly(α -methylstyrene) surfaces irradiated by excimer lasers. *J. Vac. Sci. Technol. A* **1986**, *4*, 2459–2462. [[CrossRef](#)]
188. See, T.L.; Liu, Z.; Li, L.; Zhong, X.L. A comparison of the characteristics of excimer and femtosecond laser ablation of acrylonitrile butadiene styrene (ABS). *Appl. Surf. Sci.* **2016**, *364*, 467–476. [[CrossRef](#)]
189. Tsai, Y.H.; Ho, C.Y.; Chiou, Y.J. Effect analysis of material properties of picosecond laser ablation for ABS/PVC. *Proc. SPIE* **2017**, *10449*, 69–74. [[CrossRef](#)]
190. Kim, G.D.; Rundel, J.T.; Paul, B.K. UV laser ablation of polyetherimide embossing tools for the packaging of membranes and microchannels using sealing bosses. *Int. J. Precis. Eng. Manuf.* **2010**, *11*, 665–671. [[CrossRef](#)]
191. Belaud, V.; Valette, S.; Stremdoerfer, G.; Beaugiraud, B.; Audouard, E.; Benayoun, S. Femtosecond laser ablation of polypropylene: A statistical approach of morphological data. *Scanning* **2014**, *36*, 209–217. [[CrossRef](#)] [[PubMed](#)]
192. Lutey, A.H.A.; Moroni, F. Pulsed laser texturing for improved adhesive-bonded polyethylene (PE) joints. *Int. J. Adhes. Adhes.* **2020**, *102*, 102676. [[CrossRef](#)]
193. Hu, X.; Wong, T.K.S.; Gao, S.; Liu, H.M.; Lam, Y.L.; Chan, Y.C.; Xu, F.L. Direct patterning of electro-deposited polythiophene thin films by ultraviolet laser ablation. *Proc. SPIE* **1997**, *3183*, 57–65. [[CrossRef](#)]
194. Aguilar, C.A.; Lu, Y.; Mao, S.; Chen, S. Direct micro-patterning of biodegradable polymers using ultraviolet and femtosecond lasers. *Biomaterials* **2005**, *26*, 7642–7649. [[CrossRef](#)] [[PubMed](#)]

195. Lim, Y.C.; Johnson, J.; Fei, Z.; Farson, D.F.; Lannutti, J.J.; Choi, H.W.; Lee, L.J. Micropatterning and characterization of electrospun PCL/gelatin nanofiber tissue scaffolds by femtosecond laser ablation. *ICALEO* **2009**, *2009*, 1114–1123. [[CrossRef](#)]
196. Paun, I.A.; Zamfirescu, M.; Mihailescu, M.; Luculescu, C.R.; Mustaciosu, C.C.; Dorobantu, I.; Calenic, B.; Dinescu, M. Laser micro-patterning of biodegradable polymer blends for tissue engineering. *J. Mater. Sci.* **2014**, *50*, 923–936. [[CrossRef](#)]
197. Zhang, S.; Yang, Q.; Wang, C.; Luo, X.; Kim, J.; Wang, Z.; Yamauchi, Y. Porous Organic Frameworks: Advanced Materials in Analytical Chemistry. *Adv. Sci.* **2018**, *5*, 1801116. [[CrossRef](#)] [[PubMed](#)]
198. Liu, X.; Lin, W.; Astruc, D.; Gu, H. Syntheses and applications of dendronized polymers. *Prog. Polym. Sci.* **2019**, *96*, 43–105. [[CrossRef](#)]
199. Lundin, P.M.; Fiser, B.L.; Blackledge, M.S.; Pickett, H.L.; Copeland, A.L. Functionalized Self-Assembled Monolayers: Versatile Strategies to Combat Bacterial Biofilm Formation. *Pharmaceutics* **2022**, *14*, 1613. [[CrossRef](#)]
200. Ariga, K.; Lvov, Y.; Decher, G. There is still plenty of room for layer-by-layer assembly for constructing nanoarchitectonics-based materials and devices. *PCCP* **2022**, *24*, 4097–4115. [[CrossRef](#)]
201. Singh, R.S. Langmuir and Langmuir–Blodgett films of aromatic amphiphiles. *Soft Mater.* **2022**, *20*, 57–98. [[CrossRef](#)]
202. Morallon, E.; Salavagione, H.J.; Barbero, C.A.; Acevedo, D.F.; Lasagni, A.; Mücklich, F. Metodo de Fabricacion de Superficies Metalicas Estructuradas para Usar en Espectroscopia Raman Aumentada por la Superficie y Otras Espectroscopias Relacionadas. Spain P2010000031, 1 December 2010.
203. Lasagni, A.F. Apparatus and Methods for the Interference Patterning of Planar Samples. U.S. Patent 9.233,435 B2, 12 January 2016.